

Stochastic properties of Trichel-pulse corona: A non-Markovian random point process

R. J. Van Brunt and S. V. Kulkarni

National Institute of Standards and Technology, Gaithersburg, Maryland 20899

(Received 1 June 1990)

The stochastic properties of negative, point-to-plane, Trichel-pulse corona discharges are completely characterized in terms of a set of measured conditional and unconditional discharge pulse-amplitude and pulse-time-separation distributions. The Trichel-pulse phenomenon is shown to be a clear example of a non-Markovian, marked random point process in which memory effects play an important role. Strong correlations are shown to exist among the amplitudes and time separations of successive discharge pulses that indicate how initiation and growth of a discharge pulse are affected by the presence of residual ion space charge and metastable species from previous pulses. The analysis required to assess consistency among the various measured probability distributions is discussed and used to interpret observed variations in distribution profiles. Because of the observed dependence of discharge pulse amplitude on both the amplitude of and time separation from the previous pulse, memory can propagate indefinitely back in time. The experimental limitations to verifying the extent of memory propagation are analyzed.

I. INTRODUCTION

The "regular" pulsating characteristic of negative point-to-plane corona discharges in air was first described in 1938 by Trichel.¹ The negative-corona discharge pulses that exhibit the regular relaxation oscillator behavior seen by Trichel have appropriately become known as "Trichel pulses." The phenomenon was subsequently verified by Weissler² and Loeb and co-workers³ who further characterized the discharge behavior and showed that it generally occurs in all electronegative gases but not in pure nonelectronegative gases such as nitrogen and argon. In these early works the phenomenon was reported to occur over wide ranges of voltage above discharge onset and of point-to-plane electrode gap spacing. The occurrence of Trichel pulses is also not dependent on the type of electrode material. Later investigations⁴⁻⁸ were undertaken to determine the range of conditions over which Trichel pulses appear and to measure the dependencies of their onset, amplitude, and repetition rate on such parameters as gas pressure, gap voltage, electrode spacing, and gas composition. There have also been reported measurements⁸⁻¹⁵ of the discharge pulse shape as a function of different operating conditions.

Despite the abundance of phenomenological information acquired about Trichel-pulse discharges, the process has defied a complete theoretical description. Earlier explanations^{1,3,6,16,17} of the physical mechanisms responsible for Trichel pulses were generally qualitative or semiquantitative at best. Only recently has there been some success by Morrow^{18,19} in predicting the shapes of the *first* Trichel pulses under rather restricted conditions. Morrow's model, which is an extension of earlier work by Morrow and Lowke,²⁰ is reasonably complete in the sense that it includes all of the essential continuity equations

for electron, ion, and radiation transport coupled with Poisson's equation for the electric field. It also allows for secondary-electron emission effects at the cathode.

The limitations of Morrow's model are to be found in the approximations and methods of solution required to make the calculations tractable. A one-dimensional approximation which neglects diffusion is used for the charged-particle continuity equations. Because a three-dimensional treatment of Poisson's equation is required,^{21,22} assumptions must be made about the space-charge distribution within the gap at any given time. The model has not been applied to discharge pulses that occur after the first pulse, which are often referred to in the literature as *regular* Trichel pulses. The difficulties to be encountered in using Morrow's model to describe the regular-pulse behavior should become evident from the work presented here.

It was recognized, even in the earliest investigations^{3,13} of this phenomenon, that the amplitude of the first pulse is consistently higher than that of subsequent pulses. Cross and co-workers¹³ have observed significant changes in pulse shape after the first pulse. A satisfactory explanation of differences between the first pulse and the subsequent regular pulses has not been given. It is evident, however, from the description of the discharge process given by Lama and Gallo,⁶ that, after the first pulse, the gap contains moving space-charge clouds that can perturb the electric field and thereby influence the development of the regular pulses. The influence of moving space charge could, in fact, be similar to that which is known^{23,24} to affect the recovery of Geiger counter tubes following the occurrence of a discharge pulse. Thus it can be argued from the evidence uncovered in previous investigations of Trichel pulses that the phenomenon is inherently a non-Markovian stochastic process in which

“memory effects” play an important role. The memory effects are those associated with residuals such as ion space charge or metastable species from earlier pulses that influence the onset and development of subsequent pulses.

There is evidence from the recent experimental work of Steiner²⁵ that there are strong correlations among successive Trichel pulses. Steiner, however, made no attempt to give a physical explanation for these correlations. Malik and Al-rainy²⁶ measured the statistical variations of Trichel-pulse amplitudes, but failed to obtain enough information from their data to uncover correlations among successive pulses. In our previous preliminary work on this subject^{27–30} we reported strong correlations among the amplitudes and time separations of successive Trichel pulses, but did not present a careful analysis of the possible physical mechanisms that could account for the observed correlations.

In the present work, a newly developed measurement technique²⁷ is used to obtain detailed information about the stochastic behavior of Trichel pulses in nitrogen-oxygen and neon-oxygen gas mixtures. The technique allows direct measurement of a set of *conditional* pulse-amplitude and pulse-time-separation distributions from which correlations among successive pulses can be quantitatively ascertained and related to memory effects in the discharge process. It is shown, for example, that pulse amplitude is strongly dependent on the time separation from the previous pulse and that this dependence is consistent with the influence of the moving negative-ion space charge from the previous pulse in reducing the electric field at the cathode when the next discharge pulse develops. The measured conditional distributions are not independent and are shown to satisfy a set of required consistency relationships. The stochastic properties of Trichel pulses for the two gas mixtures are found to be distinctly different. This difference is attributed to the relative importance in each gas of ion space charge versus metastable states on discharge pulse initiation and growth.

The purpose of the present work is to exhibit and interpret examples of data that reveal general features of the stochastic behavior which are relevant over wide ranges of conditions. An understanding of this stochastic behavior is shown here to be essential in any attempt to formulate a successful theoretical model for regular Trichel pulses, i.e., the model must take into account the significant influence of memory uncovered here. It is not the purpose of the present work to give a complete or precise electrical characterization of Trichel pulses for well-defined conditions as has been the subject of much of the earlier work mentioned above. The results of the present work, however, indicate the difficulties that will be encountered in attempts to make precise characterizations.

II. THEORETICAL CONSIDERATIONS

The purposes of this section are (i) to define the measurable conditional and unconditional pulse-height and

pulse-time-separation probability distributions, (ii) to discuss their properties, and (iii) to derive the consistency relationships that must be satisfied among these distributions for conditions that are relevant to Trichel pulses. The general theory of probabilities upon which this discussion is based can be found in numerous texts (see, for example, Refs. 31–33).

A. Definitions

The Trichel-pulse phenomenon can be represented by a doubly stochastic, marked random point process introduced by König and Matthes and discussed by Snyder.³³ The process is indicated diagrammatically in Fig. 1. The pulses occur at discrete times t_i and are *marked* with an amplitude q_i . The process is doubly stochastic because the evolution of the marks (pulses) and the occurrence times are influenced by an “outside” random process as well as by self-excitation from previous pulses. The outside random process in this case corresponds to ultraviolet (uv) irradiation of the cathode which, for the experimental conditions used, was required to sustain a continuous train of pulses. Although the probability for occurrence of a pulse at t_i was largely controlled by release of photoelectrons from the cathode by the uv radiation, self-excitation due to release of initiating electrons by residuals, e.g., species in metastable excited states, from previous pulses is, as shown below, significant under some conditions.

In general, both q_i and t_i depend on the set $\{q_j, t_j\}$, $j < i$, of all previous pulse amplitudes and their times of occurrence.²⁷ The Trichel-pulse phenomenon will be defined here as a stochastic process specified by a discrete, finite set $\{q_1, q_j, \Delta t_{j-1}\}_n$, $j = 2, 3, 4, \dots, n$ (see Fig. 1), where $\Delta t_{j-1} = t_j - t_{j-1}$, since pulse time separations rather than actual occurrence times are the quantities either measured or specified in the experiment. The pulse amplitude was chosen as the relevant mark because, as shown in Sec. III, it is the appropriate measure of discharge *intensity* under the experimental conditions used.

A list of the probability distributions that could be measured in the present experiment are given in Table I. The distributions p_0 are unconditional whereas the distributions p_1 and p_2 are conditional. These distributions are defined, for example, such that $p_0(q_n)dq_n$ is the probability that the n th discharge pulse in the se-

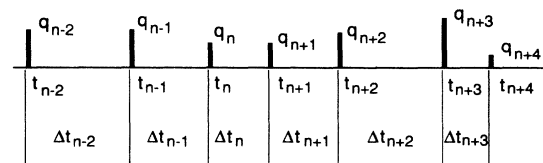


FIG. 1. Diagrammatic representation of the marked random point process corresponding to the Trichel-pulse discharge phenomenon. The Δt_n are pulse time separations and the q_n are pulse amplitudes.

TABLE I. Measurable pulse-amplitude and pulse-time-separation distributions.

Unconditional distributions	$p_0(q_n)$ $p_0(\Delta t_n)$
First-order conditional distributions	$p_1(q_n q_{n-1})$ $p_1(q_n \Delta t_{n-j}), j = 1, 2, 3, 4$ $p_1(\Delta t_n q_n)$ $p_1(\Delta t_n \Delta t_{n-1})$
Second-order conditional distributions	$p_2(q_n \Delta t_{n-1}, q_{n-1})$ $p_2(q_n \Delta t_{n-1}, \Delta t_{n-2})$

quence has an amplitude between q_n and $q_n + dq_n$, independent of previous pulse amplitudes or time separations; $p_1(q_n|\Delta t_{n-1})dq_n$ is the probability that the n th pulse has an amplitude in the same range if this pulse is separated from the previous pulse by a fixed time separation Δt_{n-1} ; and $p_2(q_n|\Delta t_{n-1}, q_{n-1})dq_n$ is the same probability, but with both Δt_{n-1} and q_{n-1} fixed. The distributions apply to arbitrary n since n was not defined by the measurement process.

All conditional and unconditional distributions, by definition, satisfy the following normalization requirement:

$$\int_0^\infty p_j(x|q_{n-1}, \Delta t_{n-1}, \dots) dx = 1, \quad (1)$$

which holds for arbitrary $j \geq 0$, where $x = q_n$ or Δt_n . It is often convenient for display purposes to use distributions that are arbitrarily normalized to the maximum value, e.g., $p_0(q_n)/p_0(q_{n,\max})$ where $q_{n,\max}$ corresponds to the maximum in $p_0(q_n)$.

B. Correlation and memory

By making a comparison of the measured conditional and unconditional pulse-height and time-separation distributions it is possible to infer immediately whether or not two random variables such as q_n and Δt_{n-1} are correlated and therefore dependent. If it is found, for example, that $p_1(q_n|\Delta t_{n-1}) \neq p_0(q_n)$ for at least some allowed values of q_n and for all allowed Δt_{n-1} such that $p_0(\Delta t_{n-1}) \neq 0$, then q_n and Δt_{n-1} are dependent variables. Likewise, if $p_2(q_n|\Delta t_{n-1}, q_{n-1}) \neq p_1(q_n|\Delta t_{n-1})$

for allowed q_{n-1} , then a dependence must exist between q_n and q_{n-1} at a fixed Δt_{n-1} .

It is found experimentally for Trichel pulses, as will be seen later, that there generally exists a significant time separation range $\Delta t_c \leq \Delta t_{n-1} \leq \Delta t_\ell$ in which the variable q_n is strongly dependent on Δt_{n-1} . The variable q_n is defined here to have a *strong dependence* on Δt_{n-1} if there is a one-to-one correspondence between the expectation value $\langle q_n(\Delta t_{n-1}) \rangle$ and Δt_{n-1} , where

$$\langle q_n(\Delta t_{n-1}) \rangle = \int_0^\infty q_n p_1(q_n|\Delta t_{n-1}) dq_n, \quad (2)$$

and where the width of $p_1(q_n|\Delta t_{n-1})$ is sufficiently small so that $q_n(\Delta t_{n-1})$ lies within a narrow range defined by $\langle q_n(\Delta t_{n-1}) \rangle \pm \delta q_n$, where $\langle q_n(\Delta t_{n-1}) \rangle \gg |\delta q_n|$ at a particular Δt_{n-1} . Under the strong dependence condition, q_n is approximately a function of Δt_{n-1} , so that

$$q_n \simeq f(\Delta t_{n-1}), \quad (3)$$

for $\Delta t_c \leq \Delta t_{n-1} \leq \Delta t_\ell$. Equation (3) suggests that $p_1(q_n|\Delta t_{n-1})$ can be represented by the approximation

$$p_1(q_n|\Delta t_{n-1}) \simeq (1 - \varepsilon)\delta(q_n - f(\Delta t_{n-1})) + \varepsilon p_0(q_n), \quad (4)$$

where $\varepsilon \ll 1$ and $\delta(q_n - f(\Delta t_{n-1}))$ is the Dirac delta function.

A measure of the degree of correlation between any two random variables x and y corresponding to any two of the measured quantities in the set $\{q_1, q_j, \Delta t_{j-1}\}_n$ is given by the *correlation coefficient* $R_{x,y}$, where

$$R_{x,y} = \frac{\int_x \int_y p_0(x) p_1(y|x) (x - \langle x \rangle) (y - \langle y \rangle) dx dy}{\left(\int_x p_0(x) (x - \langle x \rangle)^2 dx \int_y p_0(y) (y - \langle y \rangle)^2 dy \right)^{1/2}}, \quad (5)$$

which can be computed if $p_0(x)$, $p_0(y)$, and $p_1(y|x)$ have been measured. In Eq. (5), $\langle x \rangle$ and $\langle y \rangle$ are expectation (mean) values given by

$$\langle \xi \rangle = \int_\xi \xi p_0(\xi) d\xi, \quad \xi = x \text{ or } y, \quad (6)$$

where the variable x must precede y in the time sequence.

The integrals in Eqs. (5) and (6) are over all allowed values of x and y . It is seen that if x and y are uncorrelated, then $p_1(y|x) = p_0(y)$ for all allowed x and $R_{x,y} = 0$; whereas if y is strongly dependent on x over its allowed range, e.g., $y \propto x$, then it can be verified that $|R_{x,y}| \simeq 1$. In general, $|R_{x,y}| \leq 1$, where $R_{x,y} = 0$ if x and y are uncorrelated.^{31,32} If the random variable

y is *positively* dependent on x such that an increase in x implies an increase in $\langle y(x) \rangle$ such as would be given by Eq. (2), then $R_{x,y} > 0$, and if y is *negatively* dependent on x such that an increase in x implies a decrease in $\langle y(x) \rangle$, then $R_{x,y} < 0$. A positive dependence will be denoted here by $x \uparrow \Rightarrow y \uparrow$ and a negative dependence by $x \uparrow \Rightarrow y \downarrow$. The variable x can be *any* random variable that precedes y in the time sequence, e.g., $x = \Delta t_{n-j}$, for $j \geq 1$, when $y = \Delta t_n$. If x does not immediately precede y in the time ordering, then the dependence of y on x may be conditioned on assumed fixed values for intermediate variables. The signs for the dependences in this case will be denoted by $(x \uparrow \Rightarrow y \uparrow, \{\xi_i\})$ or $(x \uparrow \Rightarrow y \downarrow, \{\xi_i\})$, where $\{\xi_i\}$ is a set of *fixed* intermediate variables. For example, a positive dependence of q_n on Δt_{n-2} for fixed Δt_{n-1} is denoted by $(\Delta t_{n-2} \uparrow \Rightarrow q_n \uparrow, \{\Delta t_{n-1}\})$.

In the case of Trichel pulses, the dependence of q_n on

Δt_{n-1} is positive for $\Delta t_c \leq \Delta t_{n-1} \leq \Delta t_\ell$, i.e., $\Delta t_{n-1} \uparrow \Rightarrow q_n \uparrow$. If the pulse time separation is greater than a critical value Δt_ℓ for which residuals from previous pulses cease to influence the onset or growth of the next pulse, a *loss of memory* ensues. The correlation coefficients $R_{q_n, \Delta t_{n-1}}$ and $R_{\Delta t_n, \Delta t_{n-1}}$ diminish increasingly from unity as the fraction of time intervals above Δt_ℓ increases, i.e., as the probability

$$p(\Delta t_{n-1} > \Delta t_\ell) = \int_{\Delta t_\ell}^{\infty} p_0(\Delta t_{n-1}) d(\Delta t_{n-1}) \quad (7)$$

increases.

Another measure of the extent to which memory is important for pulse time separations in any range $t_a \leq \Delta t_n \leq t_b$ is given by the *memory coefficient* $M_1(t_a, t_b)$, defined here for first-order conditional distributions by

$$M_1(t_a, t_b) = \frac{\int_0^\infty \int_0^{t_a, b} [p_1(q|t_b - \tau) - p_1(q|t_a + \tau)]^2 d\tau dq}{\int_0^\infty \int_{t_a}^{t_b} [p_1(q|\tau)]^2 d\tau dq}, \quad (8)$$

where

$$t_{a,b} = (t_a + t_b)/2. \quad (9)$$

If memory does not exist for pulse time separations in the interval (t_a, t_b) , such that $p_1(q|t_b - \tau) = p_1(q|t_a + \tau)$ for all $0 \geq \tau \geq t_{a,b}$, then $M_1(t_a, t_b) = 0$, whereas $M_1(t_a, t_b) \neq 0$ implies the existence of some memory. It is required for a meaningful definition of $M_1(t_a, t_b)$ that $p_1(q|\tau) \neq 0$ in at least some subinterval $(t'_a, t'_b) \in (t_a, t_b)$ where $t'_a \geq t_a, t'_b \geq t_b$. The conditional distribution p_1 in Eq. (8) can be any $p_1(q_n|\Delta t_{n-j})$ or $p_1(\Delta t_n|\Delta t_{n-j})$ for $j < n$. The advantage of the memory coefficient over the correlation coefficient is that the former applies over a restricted time-separation range whereas the latter is evaluated for the entire range of allowed separations. Memory coefficients can also be defined in terms of higher-order conditional distributions $p_j, j > 1$.

C. Integral relationships among measured distributions

If memory is important in the stochastic process, then the distributions listed in Table I are not independent, e.g., the behavior of the time-interval distribution $p_0(\Delta t_n)$ affects the shape of the pulse-amplitude distribution $p_0(q_n)$ and vice versa. It can be shown from the law of probabilities^{31,32} that the measured distributions must satisfy the following integral relationships:

$$p_0(q_n) = \int_0^\infty p_0(\Delta t_{n-1}) p_1(q_n|\Delta t_{n-1}) d(\Delta t_{n-1}), \quad (10)$$

$$p_0(q_n) = \int_0^\infty p_0(\Delta t_{n-j}) p_1(q_n|\Delta t_{n-j}) d(\Delta t_{n-j}), \quad j > 1, \quad (11)$$

$$p_0(q_n) = \int_0^\infty p_0(q_{n-1}) p_1(q_n|q_{n-1}) dq_{n-1}, \quad (12)$$

$$p_0(\Delta t_n) = \int_0^\infty p_0(q_n) p_1(\Delta t_n|q_n) dq_n, \quad (13)$$

$$p_1(q_n|\Delta t_{n-1}) = p_0(\Delta t_{n-1})^{-1} \times \int_0^\infty p_0(q_{n-1}) p_1(\Delta t_{n-1}|q_{n-1}) \times p_2(q_n|q_{n-1}, \Delta t_{n-1}) dq_{n-1}, \quad (14)$$

$$p_1(q_n|q_{n-1}) = \int_0^\infty p_1(\Delta t_{n-1}|q_{n-1}) \times p_2(q_n|q_{n-1}, \Delta t_{n-1}) d(\Delta t_{n-1}). \quad (15)$$

From Eqs. (10), (12), (14), and (15) it is seen that

$$p_0(q_n) = \int_0^\infty \int_0^\infty p_0(q_{n-1}) p_1(\Delta t_{n-1}|q_{n-1}) \times p_2(q_n|q_{n-1}, \Delta t_{n-1}) dq_{n-1} d(\Delta t_{n-1}). \quad (16)$$

The evaluation of the integrals in Eqs. (10)–(16) serves as a check on the self-consistency of the measured distributions.

In addition to the above integrals, there are other useful integral relationships that apply if the strong dependency condition between q_n and Δt_{n-1} is valid. Another expression for $p_1(q_n|\Delta t_{n-1})$ from the law of probabilities is

$$p_1(q_n|\Delta t_{n-1}) = p_0(\Delta t_{n-1})^{-1} \int_0^\infty \int_0^\infty p_0(\Delta t_{n-2}) p_1(q_{n-1}|\Delta t_{n-2}) \\ \times p_2(\Delta t_{n-1}|q_{n-1}, \Delta t_{n-2}) p_3(q_n|q_{n-1}, \Delta t_{n-1}, \Delta t_{n-2}) d(\Delta t_{n-2}) dq_{n-1}. \quad (17)$$

Using the strong dependency condition, Eq. (3), and the normalization requirement, Eq. (1), it can be shown that Eq. (17) becomes

$$p_1(q_n|\Delta t_{n-1}) \simeq p_0(\Delta t_{n-1})^{-1} \int_0^\infty p_0(\Delta t_{n-2}) p_1(\Delta t_{n-1}|\Delta t_{n-2}) p_2(q_n|\Delta t_{n-1}, \Delta t_{n-2}) d(\Delta t_{n-2}). \quad (18)$$

From similar arguments, the following also hold for a strong $(q_n, \Delta t_{n-1})$ dependence:

$$p_1(\Delta t_n|\Delta t_{n-1}) \simeq \int_0^\infty p_1(\Delta t_n|q_n) p_1(q_n|\Delta t_{n-1}) dq_n, \quad (19)$$

$$p_1(q_n|\Delta t_{n-2}) \simeq \int_0^\infty p_1(\Delta t_{n-1}|\Delta t_{n-2}) p_2(q_n|\Delta t_{n-1}, \Delta t_{n-2}) d(\Delta t_{n-1}), \quad (20)$$

$$p_2(q_n|\Delta t_{n-1}, \Delta t_{n-2}) \simeq p_1(\Delta t_{n-1}|\Delta t_{n-2})^{-1} \int_0^\infty p_1(q_{n-1}|\Delta t_{n-2}) p_1(\Delta t_{n-1}|q_{n-1}) p_2(q_n|q_{n-1}, \Delta t_{n-1}) dq_{n-1}. \quad (21)$$

Equations (10)–(21) are used here to understand the profiles of measured distributions and to derive consistency relationships in the signs of correlations among successive pulse amplitudes and time separations.

D. Consistency among $p_1(q_n|\Delta t_{n-1})$, $p_1(\Delta t_n|\Delta t_{n-1})$, and $p_1(\Delta t_n|q_n)$

The integral relationships in the Sec. II C imply a certain consistency of behavior among the first-order conditional distributions $p_1(q_n|\Delta t_{n-1})$, $p_1(\Delta t_n|q_n)$, and $p_1(\Delta t_n|\Delta t_{n-1})$ with respect to the implied signs of the dependences between the pairs of random variables $(q_n, \Delta t_{n-1})$, $(\Delta t_n, q_n)$, and $(\Delta t_n, \Delta t_{n-1})$. This consistency applies for monotonic dependences, i.e., dependences between random variables that do not change sign, and for the case of a strong positive dependence of q_n on Δt_{n-1} , thus implying that Eq. (19), which relates the above distributions, can be considered. By using Eq. (4) in Eq. (19) it can be verified that $(\Delta t_{n-1} \uparrow \Rightarrow q_n \uparrow)$ plus $(q_n \uparrow \Rightarrow \Delta t_n \uparrow)$ gives $(\Delta t_{n-1} \uparrow \Rightarrow \Delta t_n \uparrow)$ as the required behavior for $p_1(\Delta t_n|\Delta t_{n-1})$. According to Eq. (19) for this case, an increase in the value of Δt_{n-1} implies an increase in the expectation value $\langle \Delta t_n(\Delta t_{n-1}) \rangle$. Likewise it is found from Eq. (19) that $(\Delta t_{n-1} \uparrow \Rightarrow q_n \uparrow)$ plus $(q_n \uparrow \Rightarrow \Delta t_n \downarrow)$ requires $(\Delta t_{n-1} \uparrow \Rightarrow \Delta t_n \downarrow)$. Both cases have been observed here to occur for Trichel pulses.

It should also be noted that if there is a lack of correlation between Δt_n and q_n , then $p_1(\Delta t_n|q_n) = p_0(\Delta t_n)$ for all allowed q_n and Eq. (19) gives $p_1(\Delta t_n|\Delta t_{n-1}) = p_0(\Delta t_n)$. This means that a lack of dependence of Δt_n on q_n requires a lack of dependence of Δt_n on Δt_{n-1} if the strong dependency condition between q_n and Δt_{n-1} applies.

E. Consistency among $p_1(q_n|\Delta t_{n-1})$, $p_2(q_n|\Delta t_{n-1}, q_{n-1})$, and $p_2(q_n|\Delta t_{n-1}, \Delta t_{n-2})$

As in the case of the first-order conditional time-interval distributions discussed in Sec. II D, a strong positive

dependence of q_n on Δt_{n-1} requires that the dependencies between the pairs (q_n, q_{n-1}) and $(q_n, \Delta t_{n-2})$ for fixed Δt_{n-1} be of the same sign. This can be shown using Eq. (3) in Eq. (21). Given the signs of the $(q_n, \Delta t_{n-1})$ and (q_n, q_{n-1}) dependences, the sign of the $(q_n, \Delta t_{n-2})$ dependence can be ascertained by examining the changes in weighting of q_{n-1} and q_n when Δt_{n-2} is changed as implied by the first and third terms in the product forming the integrand for Eq. (21) at fixed Δt_{n-1} . The terms $p_1(\Delta t_{n-1}|\Delta t_{n-2})^{-1}$ and $p_1(\Delta t_{n-1}|q_{n-1})$ affect only the magnitude of the integral in Eq. (21) and not the weighting of q_{n-1} and q_n values. For fixed Δt_{n-1} , $(\Delta t_{n-2} \uparrow \Rightarrow q_{n-1} \uparrow)$ plus $(q_{n-1} \uparrow \Rightarrow q_n \uparrow, \{\Delta t_{n-1}\})$ requires $(\Delta t_{n-2} \uparrow \Rightarrow q_n \uparrow, \{\Delta t_{n-1}\})$. Likewise, $(\Delta t_{n-2} \uparrow \Rightarrow q_{n-1} \uparrow)$ plus $(q_{n-1} \uparrow \Rightarrow q_n \downarrow, \{\Delta t_{n-1}\})$ requires $(\Delta t_{n-2} \uparrow \Rightarrow q_n \downarrow, \{\Delta t_{n-1}\})$. Both cases are shown here to occur for Trichel pulses. It can also be shown that a lack of dependence of q_n on Δt_{n-2} at fixed Δt_{n-1} implies a lack of dependence of q_n on q_{n-1} if the strong $(q_{n-1}, \Delta t_{n-2})$ dependency condition holds.

It should be noted that the physical bases for the (q_n, q_{n-1}) and $(q_n, \Delta t_{n-2})$ dependences are not the same as for the $(\Delta t_n, q_n)$ and $(\Delta t_n, \Delta t_{n-1})$ dependences considered in Sec. II D. The dependence of Δt_n on q_n is related to the effect of residuals from the n th pulse on the *initiation* of the subsequent pulse, whereas the dependence of q_n on q_{n-1} is related to the effect of residuals from the $(n-1)$ st pulse on the *growth* of the subsequent pulse.

From Eq. (20), which applies for a strong $(q_n, \Delta t_{n-1})$ dependence, it can be seen that correlations between Δt_{n-1} and Δt_{n-2} or between q_n and Δt_{n-2} for fixed Δt_{n-1} , implied respectively by $p_1(\Delta t_{n-1}|\Delta t_{n-2})$ and $p_2(q_n|\Delta t_{n-1}, \Delta t_{n-2})$, lead to a dependence of q_n on Δt_{n-2} independent of Δt_{n-1} . For uv-sustained Trichel pulses, the effects of the two correlations implied by p_1 and p_2 in Eq. (20) can either reinforce or counteract each other so that the sign of the $(q_n, \Delta t_{n-2})$ dependence determined by $p_1(q_n|\Delta t_{n-2})$ depends on the relative signs and strengths of the $(\Delta t_{n-1}, \Delta t_{n-2})$ dependence and the

$(q_n, \Delta t_{n-2})$ dependence for fixed Δt_{n-1} . For a strong $(q_n, \Delta t_{n-1})$ dependence, Eq. (15) implies that Eq. (20) is a good approximation, and therefore, the behavior of $p_1(q_n|\Delta t_{n-2})$ should be like that for $p_1(q_n|q_{n-1})$, e.g., $(\Delta t_{n-2} \uparrow \Rightarrow q_{n-1} \uparrow)$ plus $(q_{n-1} \uparrow \Rightarrow q_n \downarrow)$ implies $(\Delta t_{n-2} \uparrow \Rightarrow q_n \downarrow)$.

It should be emphasized that the above arguments about consistency of the signs apply only if the dependences are monotonic, namely that they do not change sign within the ranges of allowed values for the random variables considered. Although the signs of dependences between the random variables considered above can change, statistically significant changes were not found to occur in the data presented here.

F. Propagation and loss of memory (deviations from Markovian behavior)

Extending the arguments in Sec. II E, it can be shown that if q_n is dependent on *both* q_{n-1} and Δt_{n-1} for *all* arbitrary n , then in general,

$$p_j(q_n|\{\Delta t_{n-i}\}_{j-1}, \Delta t_{n-j}) \neq p_j(q_n|\{\Delta t_{n-i}\}_{j-1}, \Delta t'_{n-j}), \quad i = 1, 2, \dots, j-1, \quad (22)$$

whenever $\Delta t_{n-j} \neq \Delta t'_{n-j}$, for any $j \geq 1$. If all the time separations in the set $\{\Delta t_{n-i}\}_{j-1}$ have *fixed* values less than Δt_ℓ , then the following can be shown, in the case of monotonic correlations.

(a) $(\Delta t_{n-1} \uparrow \Rightarrow q_n \uparrow) + (q_{n-1} \uparrow \Rightarrow q_n \downarrow)$ implies

$$(\Delta t'_{n-j} \uparrow \Rightarrow q_n \uparrow, \{\Delta t_{n-i}\}_{j-1}) \text{ for odd } j$$

$$(\Delta t'_{n-j} \uparrow \Rightarrow q_n \downarrow, \{\Delta t_{n-i}\}_{j-1}) \text{ for even } j.$$

(b) $(\Delta t_{n-1} \uparrow \Rightarrow q_n \uparrow) + (q_{n-1} \uparrow \Rightarrow q_n \uparrow)$ implies

$$(\Delta t'_{n-j} \uparrow \Rightarrow q_n \uparrow, \{\Delta t_{n-i}\}_{j-1}) \text{ for all } j.$$

The existence of dependences between both of the pairs $(q_j, \Delta t_{j-1})$ and (q_j, q_{j-1}) therefore allows memory to propagate indefinitely back in time provided $\Delta t_j < \Delta t_\ell$ for all values of j . A dependence of Δt_n on q_n can also influence memory propagation. Memory will cease beyond the first event to have a time separation from the previous event greater than the critical minimum time separation Δt_ℓ for which $M_1(\Delta t_\ell, \Delta t_u) = 0$, where Δt_u is any time separation greater than Δt_ℓ .

For the Trichel-pulse phenomenon, the initiation and growth of any discharge pulse is expected to depend overwhelmingly on residuals from the most recent previous pulse. From this consideration it has been erroneously suggested²⁷ that memory does not extend back beyond the most recent event. The above analysis indicates that, because of correlations between both $(q_j, \Delta t_{j-1})$ and (q_j, q_{j-1}) , memory can extend back beyond the most recent event even though there may be no residuals present from pulses prior to this event. If residuals

such as metastable species are present from earlier events, then they may have second-order effects on the onset and growth of a discharge pulse. It was not possible in the present experiments to distinguish contributions to memory from such second-order effects. It is assumed here that "memory" results predominantly from the dependences of q_n (or Δt_n) on q_{n-1} and Δt_{n-1} .

It is evident from the above discussion that the Trichel-pulse phenomenon is not a Markov process. By definition,^{27,33} a Markov process, jointly defined for the two random variables q_i and Δt_{i-1} , requires

$$p_{2j+1}(q_n|\Delta t_{n-1}, \{q_i, \Delta t_{i-1}\}_j) = p_2(q_n|q_{n-1}, \Delta t_{n-1}), \quad (23)$$

$i = n-1, n-2, \dots, n-j$ for all $j \leq n-1$.

If q_i is strongly dependent on Δt_{i-1} , then

$$p_{2j+1}(q_n|\Delta t_{n-1}, \{q_i, \Delta t_{i-1}\}_j) \simeq p_{j+1}(q_n|\Delta t_{n-1}, \{\Delta t_{i-1}\}_j). \quad (24)$$

In this case, the Markov requirement becomes

$$p_{2j+1}(q_n|\Delta t_{n-1}, \{\Delta t_{i-1}\}_j) = p_1(q_n|\Delta t_{n-1}), \quad j \leq n-1. \quad (25)$$

Obviously this is not consistent with Eq. (22). Also, if memory does not extend beyond the most recent event, it is required that

$$p_1(q_n|\Delta t_{n-j}) = p_0(q_n) \quad (26)$$

for all $j > 1$. It is shown here experimentally for Trichel pulses that, in general,

$$p_2(q_n|\Delta t_{n-1}, \Delta t_{n-2}) \neq p_1(q_n|\Delta t_{n-1}) \quad (27)$$

and

$$p_1(q_n|\Delta t_{n-j}) \neq p_0(q_n), \quad j = 2, 3, 4. \quad (28)$$

III. EXPERIMENTAL METHOD

The method used to measure the distributions given in Table I has previously been described in detail by Van Brunt and Kulkarni.²⁷ A diagram of the measurement system is shown in Fig. 2. Some modifications of the system described in Ref. 27 have been made to (i) allow direct measurement of the distributions $p_1(q_n|\Delta t_{n-j})$, $j > 2$, and $p_2(q_n|\Delta t_{n-1}, \Delta t_{n-2})$; (ii) eliminate intermediate pulse errors associated with measurement of the p_2 distributions; and (iii) reduce background associated with accidental sampling of the tails of discharge pulses.

By appropriate positioning of the switches (S1-S6) shown in Fig. 2, it is possible to configure the system to measure any of the indicated distributions. Data from all measurement configurations are accumulated by a 256-channel, computer-controlled multichannel analyzer (MCA) which uses an analog-to-digital converter to mea-

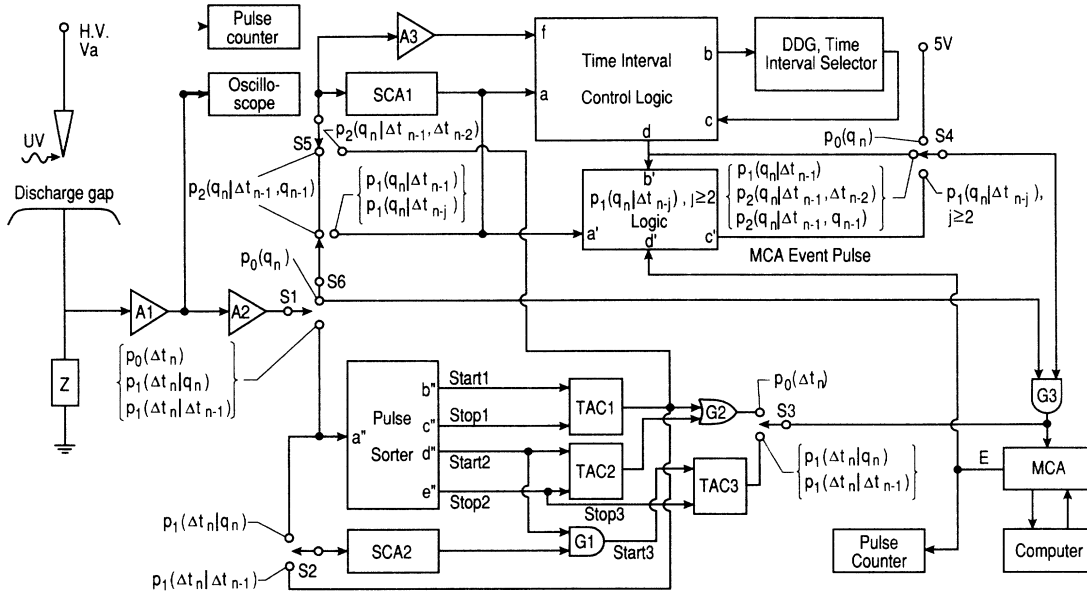


FIG. 2. System for measuring various indicated pulse-amplitude and time-separation distributions. In this diagram, the relevant components are identified as follows: MCA, multichannel analyzer; TAC, time-to-amplitude converter; SCA, single channel analyzer; DDG, digital-delay generator; A, amplifier; G, gate; and S, switch. Additional details about the individual circuits used in this system can be found in Ref. 27.

sure pulse heights.

The corona-discharge current pulses are detected electrically using a preamplifier (A1) connected to an impedance Z in series with the discharge gap. The detected pulses are then sent to a variable gain amplifier (A2) before being routed to the required circuit path for measurement of a particular distribution as determined by the position of S1. For measurement of $p_0(q_n)$, the discharge pulses from A2 are fed directly to the MCA through gate G3, which is kept permanently open by the proper positioning of S4.

The distribution $p_0(\Delta t_n)$ is measured by sending the pulses from A2 to a pulse sorter used to trigger two time-to-amplitude converters (TAC1 and TAC2) which generate output pulses of amplitude proportional to the time between the trigger pulses at the start and stop inputs. The outputs of TAC1 and TAC2 are fed to the MCA through gate G2 by appropriate positioning of S3. As shown in Ref. 27, this arrangement permits the recording of every sequential time interval, provided all time separations exceed the TAC reset time of $50 \mu\text{s}$.

The measurement of $p_1(q_n|\Delta t_{n-1})$ requires the use of a logic-controlled digital-delay generator (DDG), which restricts transfer of pulses from A2 to the MCA through G3 to a narrow, preselected time range $\Delta t_{n-1} - \delta(\Delta t_{n-1})/2$ to $\Delta t_{n-1} + \delta(\Delta t_{n-1})/2$ for which $\Delta t_{n-1} \gg \delta(\Delta t_{n-1})$, provided no intermediate pulses appear before this time window. To measure $p_2(q_n|\Delta t_{n-1}, q_{n-1})$, a single-channel analyzer (SCA1) is inserted between A2 and the input to the DDG time-interval control logic circuit by proper positionings of S1, S5, and S6. The SCA1 restricts triggering of the DDG to pulses having amplitudes within

the selected range $q_{n-1} - \delta(q_{n-1})/2$ to $q_{n-1} + \delta(q_{n-1})/2$ for which $q_{n-1} \gg \delta(q_{n-1})$. To ensure, in the case of p_2 measurements, that the time-interval control logic properly inhibits the opening of G3 if intermediate pulses occur before the selected time window, it is necessary to modify the circuit previously described²⁷ by adding the amplifier A3 with input at f . This amplifier is identical to that defined by transistor T_1 in Fig. 2 of Ref. 27. In the present configuration, the input f is connected directly to the delay τ_1 of Fig. 2 (Ref. 27) which has, in turn, been disconnected from T_1 .

Unlike the system previously described,²⁷ the present system allows direct measurement of $p_2(q_n|\Delta t_{n-1}, \Delta t_{n-2})$. For measurement of this distribution, the switches S1 and S5 are positioned so that the input to SCA1 is derived from TAC1. The time interval measured by TAC1 is restricted by SCA1 to lie within a narrow range $\Delta t_{n-2} - \delta(\Delta t_{n-2})/2$ to $\Delta t_{n-2} + \delta(\Delta t_{n-2})/2$ for triggering the DDG, which, in turn, defines Δt_{n-1} .

By the indicated positionings of switches S1, S2, and S3, it is possible to measure the conditional pulse time-separation distributions $p_1(\Delta t_n|\Delta t_{n-1})$ and $p_1(\Delta t_n|q_n)$. For measurement of $p_1(\Delta t_n|\Delta t_{n-1})$, the output of TAC1 is fed to the input of the single-channel analyzer SCA2 which thus defines Δt_{n-1} and triggers TAC3 for the measurement of the next time interval Δt_n . In the case of the $p_1(\Delta t_n|q_n)$ measurement, SCA2 is connected directly to amplifier A2 thereby used to define q_n .

The present system also differs from that previously described in that the $p_1(q_n|\Delta t_{n-j})$ logic circuit now contains a pulse counter that can be set for any $j \geq 2$. By making adjustments in the delays inherent to the time-

interval control logic combined with minor adjustments in the shape of the gate pulse from this circuit which controls G3, it has been possible to largely eliminate the background problem illustrated by Fig. 5 of Ref. 27.

In the present measurement system, the pulse detection-circuit conditions are similar to those described in Ref. 7 so that the measured discharge-pulse amplitude is proportional to the net charge transported in the discharge given by

$$Q'_n = \int_{-\infty}^{\infty} i_n(t) dt, \quad (29)$$

where $i_n(t)$ is the instantaneous discharge current at time t for the n th pulse. Given the impulse response $h(t-t')$ of the detection circuit (defined here mainly by the filter characteristics of Z and A1), the observed pulse signal is given by

$$q'_n(t) = \int_{-\infty}^t i_n(t') h(t-t') dt'. \quad (30)$$

The impulse response in the present measurement system has a width w_i of about $1.5 \mu\text{s}$, whereas the intrinsic width w_p of a typical Trichel pulse is known¹²⁻¹⁵ to be on the order of 10–50 ns. Therefore the condition $w_i \gg w_p$ allows the approximation

$$i_n(t) \simeq Q'_n \delta(t-t_n), \quad (31)$$

where $\delta(t-t_n)$ is the Dirac delta function. Using this in Eq. (30) gives

$$q'_n(t) = Q'_n h(t-t_n). \quad (32)$$

This means that the shapes of the observed Trichel pulses in the present experiment are governed primarily by the shape of $h(t-t_n)$ and thus the maximum of $q'_n(t)$, denoted here by q_n , is directly proportional to Q'_n . Therefore q_n can be expressed in units of charge, and in the present case, it is convenient to use picocoulombs (pC). The method for calibrating the pulse-height measurements in terms of charge is the same as described previously.⁷

The Trichel pulses are generated by applying a dc voltage to a point-to-plane electrode gap in which the point electrode serves as the cathode. General features of the stochastic behavior reported here were found to apply over wide ranges of gap spacings, point-electrode radius, gas pressure, and gas composition. In order to achieve discharge characteristics that were constant over long periods of time (several hours) and to gain control over the rate of pulse initiation, the discharge was primarily sustained by uv irradiation from a mercury arc lamp of highly polished stainless-steel point cathodes in controlled gas mixtures. It was noted, however, that similar stochastic behavior often occurs when the discharge becomes self-sustaining or is sustained by field emission, i.e., by the Fowler-Nordheim effect,³⁴ which occurs when very sharp electrodes are used. Point-to-plane gap spacings in the range of 1.0–2.5 cm were used with points having radii of curvature at the tip in the approximate

range 0.09–0.15 mm. The gas mixtures were prepared in a metal discharge chamber after it was evacuated to a pressure of about 1×10^{-2} Torr (~ 1.3 Pa). The results presented here were obtained using the gas mixtures $\text{N}_2 + 20\% \text{O}_2$, $\text{Ne} + 5\% \text{O}_2$, $\text{Ne} + 95\% \text{O}_2$, all at an absolute total pressure of 760 Torr (~ 100 kPa).

When measurements were made of the conditional distributions (p_1 's and p_2 's of Table I) for a fixed set of discharge conditions defined by applied gap voltage, uv intensity, electrode spacing, and gas composition, it was necessary to periodically monitor the distributions $p_0(q_n)$ and $p_0(\Delta t_n)$ to ensure that there was no significant drift in these conditions. As shown in Sec. IV, the profiles for these distributions are very sensitive indicators of variations in the discharge operating conditions.

It was generally possible to maintain acceptably constant discharge conditions over a period of several hours. On the other hand, due to an inability to make sufficiently precise adjustments of the operating conditions in the present experimental setup, it was not always possible to achieve exactly the same profiles for $p_0(q_n)$ and $p_0(\Delta t_n)$ from one day to the next. This difficulty was also noted by Malik and Al-rainy.²⁶ However, for the purposes of the present work, which are not to make a precise characterization of the phenomena but rather to investigate its stochastic properties, which, as noted above, apply over wide ranges of conditions, it was not necessary to achieve exact replications of $p_0(q_n)$ and $p_0(\Delta t_n)$. The results presented here, in fact, clearly indicate that because of strong memory effects associated with the stochastic behavior of Trichel pulses, it can be expected that difficulties will be encountered in attempts to establish highly reproducible conditions.

IV. RESULTS AND DISCUSSION

Data obtained for the different distributions given in Table I are presented here. Consistency among the measured distributions is analyzed and at the end of each subsection their behavior is interpreted in terms of expected physical processes that can occur in the discharge.

A. Behavior of the unconditional distributions $p_0(q_n)$ and $p_0(\Delta t_n)$

Shown in Figs. 3 and 4 are examples of data for the unconditional pulse-amplitude and time-separation distributions at different applied gap voltages V_a for a $\text{N}_2 + 20\% \text{O}_2$ gas mixture. The data in Fig. 3 were obtained using a higher relative uv intensity to irradiate the cathode than applies to the data in Fig. 4. The discharge conditions were otherwise the same. For convenience of display, the distributions shown in these figures are normalized to the maximum values.

At "high" uv irradiation, the $p_0(q_n)$ distribution is seen in Fig. 3 to broaden with increasing V_a while $p_0(\Delta t_n)$ becomes more narrow and shifts downward. The expectation values for q_n and Δt_n given by

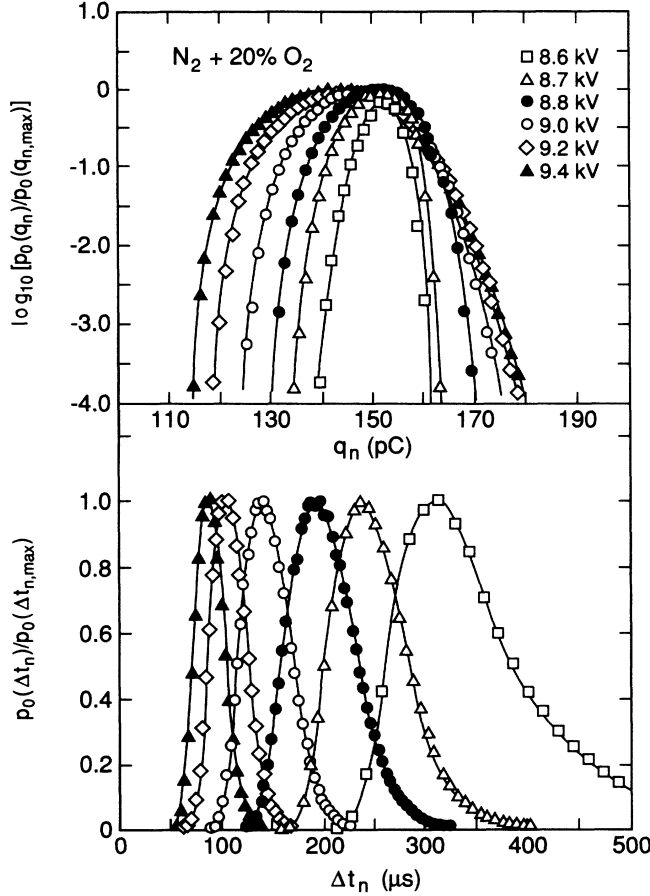


FIG. 3. Measured unconditional pulse-amplitude $p_0(q_n)$ and corresponding pulse-time-separation $p_0(\Delta t_n)$ distributions at the different indicated gap voltages, for relatively intense uv irradiation of the cathode in a 100-kPa $N_2 + 20\% O_2$ gas mixture. The distributions have been normalized to the maximum values.

$$\langle q_n \rangle = \int_0^{\infty} q_n p_0(q_n) dq_n \quad (33)$$

and

$$\langle \Delta t_n \rangle = \int_0^{\infty} \Delta t_n p_0(\Delta t_n) d(\Delta t_n) \quad (34)$$

both decrease as V_a increases. At “low” uv intensity, the data in Fig. 4 indicate that $\langle q_n \rangle$ now increases for increasing V_a while $\langle \Delta t_n \rangle$ again decreases. Also at low uv intensity, $p_0(q_n)$ becomes sharply peaked at the high end of the distribution. Contrary to suggestions from earlier work,²⁶ the distributions $p_0(q_n)$ are, in general, asymmetric and therefore distinctly non-Gaussian.

The decrease in both $\langle q_n \rangle$ and $\langle \Delta t_n \rangle$ with increasing V_a has been reported previously^{6,8,26} for “self-sustained” Trichel-pulse discharges in air and oxygen. The self-sustained discharge condition (which may be at least partially sustained by field emission at the cathode) is similar to the high uv intensity case considered here. These situations are similar in the sense that electron-emission

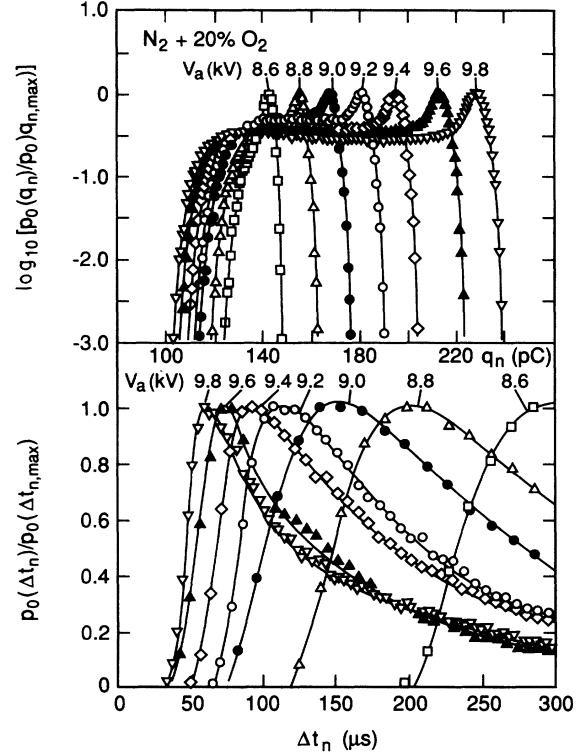


FIG. 4. Measured unconditional pulse-amplitude $p_0(q_n)$ and corresponding pulse-time-separation $p_0(\Delta t_n)$ distributions at the different indicated gap voltages, for relatively weak uv irradiation of the cathode in a 100-kPa $N_2 + 20\% O_2$ gas mixture. The distributions have been normalized to the maximum values.

rates that govern the pulse-initiation rates are high in both cases. The values for $\langle q_n \rangle$ implied by the $p_0(q_n)$ distributions in Fig. 3 are consistent in magnitude with the results of Lama and Gallo for air extrapolated to the point electrode radius used in the present experiments that exceeds their largest by a factor of 2 (see Fig. 11 of Ref. 6). The pulse repetition rates implied by the $p_0(\Delta t_n)$ distributions are also consistent in magnitude with earlier results for air.⁴⁻⁶

Figure 5 shows results for $p_0(q_n)$ and $p_0(\Delta t_n)$ obtained for different uv intensities I_i at a fixed V_a , where $I_1 > I_2 > I_3 > \dots$. The gas and electrode-gap conditions are nearly identical to those that apply for the data in Figs. 3 and 4. It is seen from Fig. 5 that the profiles for $p_0(q_n)$ and $p_0(\Delta t_n)$ are very sensitive to uv intensity. Both $\langle q_n \rangle$ and $\langle \Delta t_n \rangle$ increase with decreasing I_i . When $\langle \Delta t_n \rangle$ exceeds about 400 μ s, as implied by the $p_0(\Delta t_n)$ data in Fig. 5 for I_6 , $p_0(q_n)$ becomes very narrow and assumes a constant, nearly Gaussian shape for which $\langle q_n \rangle$ approaches a limiting maximum value, denoted here by q_{lim} .

The time-separation distributions exhibit a limiting critical minimum value Δt_c which is nearly independent of I_i . As seen in Fig. 6, Δt_c decreases with increasing voltage, consistent with results previously reported by

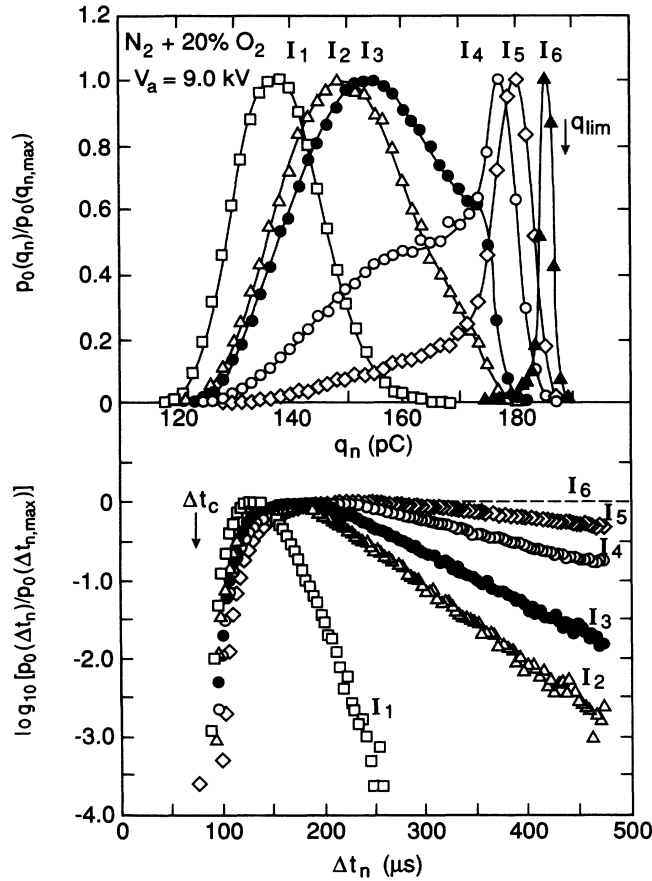


FIG. 5. Measured unconditional pulse-amplitude $p_0(q_n)$ and corresponding pulse-time-separation $p_0(\Delta t_n)$ distributions at the different indicated relative intensities of uv irradiation I_i ($I_1 > I_2 > I_3 \dots$) for a gap voltage of 9.0 kV in a 100-kPa $N_2 + 20\% O_2$ gas mixture. The distributions have been normalized to the maximum values.

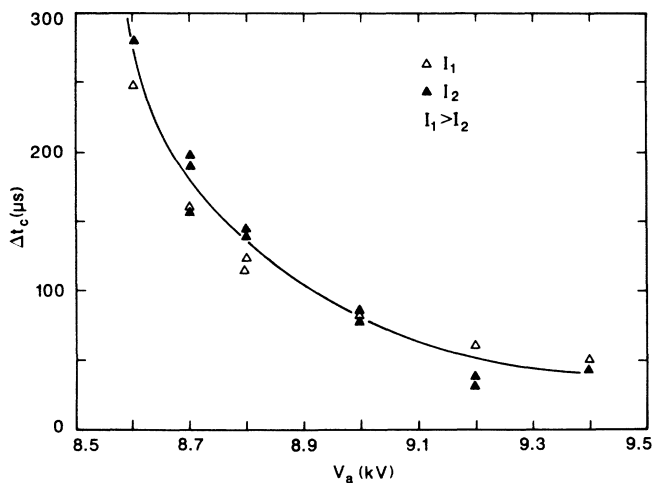


FIG. 6. Measured dependence of the critical minimum pulse separation time Δt_c on applied gap voltage for two different intensities of uv irradiation. The Δt_c were determined from data similar to those shown in Figs. 3 and 4.

Mason and Young.³⁵ This limiting time interval can be identified with the time required for restoration of the electric field near the cathode to the critical value required for initiation and growth of the next discharge pulse. This time is governed by the ambipolar diffusion of positive and negative ions away from the point.^{6,8,17} It can be expected that Δt_c should decrease with increasing V_a since the rate of ion diffusion will be enhanced as the applied field increases. Provided the ion-diffusion rate does not depend significantly upon the magnitude of q_n within the range defined by the $p_0(q_n)$'s in Fig. 5, it can be expected that Δt_c will not change significantly with I_i . The present results suggest that Δt_c is a more well-defined characteristic of the discharge than the previously measured pulse frequency⁴⁻⁶ given by $1/\langle \Delta t_n \rangle$.

The $p_0(\Delta t_n)$ distributions shown in Fig. 5 exhibit an exponential decrease for $\Delta t_n > \Delta t_{n,max}$ at a rate $d[\log_{10} p_0(\Delta t_n)]/d(\Delta t_n)$, which is proportional³⁶ to I_i . This type of behavior is expected if the probability for discharge-pulse initiation at any time after field restoration is proportional to the rate of photoelectron release from the cathode, which is, in turn, proportional to I_i . The probability for initiation of the $(n+1)$ st pulse at a time separation $\Delta t_n > \Delta t_{n,max}$ from the previous pulse can be expressed as

$$p_0(\Delta t_n) d(\Delta t_n) \approx \gamma(V_a) I_i \left(1 - \int_0^{\tau_n} p_0(\Delta t'_n) d(\Delta t'_n) \right) d(\Delta t_n), \quad (35)$$

where $\tau_n = \Delta t_n - \Delta t_{n,max}$, $\gamma(V_a)$ is a factor that depends here only on V_a , and the quantity in large parentheses represents the probability that a discharge pulse will not have been initiated for intervals in the range $\Delta t_{n,max}$ to Δt_n . The function that satisfies Eq. (35) is of the form

$$p_0(\Delta t_n) = \gamma(V_a) I_i \exp[-\gamma(V_a) I_i (\Delta t_n - \Delta t_{n,max})], \quad (36)$$

from which it is seen that

$$d[\log_{10} p_0(\Delta t_n)]/d(\Delta t_n) \propto -I_i, \quad (37)$$

consistent with the behavior for $p_0(\Delta t_n)$ exhibited in Fig. 5. This is identical to the Poisson distribution law for time lags in the electrical breakdown of gases first noted by von Laue.³⁷

The factor $\gamma(V_a)$ is included in Eq. (35) because the electric-field magnitude at the cathode is sufficiently high [often in excess of 10^5 V/cm as estimated using Eq. (40) of Sec. IV B] that the electron-release process is expected to be a *field-assisted* photoelectron emission, which is a well-known effect that has been observed experimentally³⁸ and is the optical analog of the Schottky effect³⁹ for thermionic emission from a cathode. The $p_0(\Delta t_n)$ data in Fig. 3 indicate that $\gamma(V_a)$ increases with V_a as expected. Because of this effect, perturbations of the field at the cathode due to ion space charge from pre-

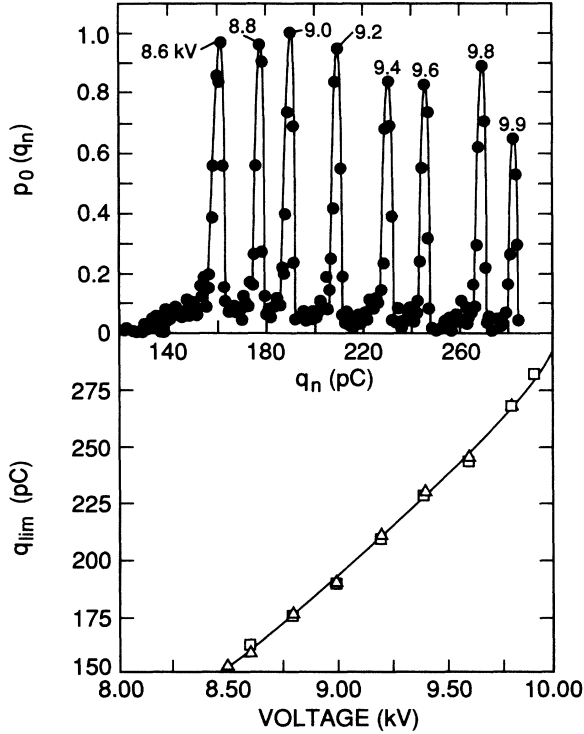


FIG. 7. Measured unconditional pulse-amplitude $p_0(q_n)$ distributions at the indicated gap voltages for very weak uv irradiation of the cathode in a 100-kPa $N_2 + 20\% O_2$ gas mixture (top), and corresponding q_{lim} vs applied gap voltage (bottom), where the q_{lim} values are associated with the maxima in the $p_0(q_n)$ distributions shown in the top portion of the figure.

vious pulses might also have an influence on the probability of electron emission. Although such an effect appears to be relatively small for the N_2-O_2 case shown in Fig. 5, results presented later demonstrate that it is significant in other gas mixtures. If space charge from a previous pulse influences the rate of electron emission, then γ will depend on q_n and Δt_{n-1} . In this case, positive correlations between Δt_n and q_n (or Δt_{n-1}) become evident from the conditional distribution $p_1(\Delta t_n|q_n)$ [or $p_1(\Delta t_n|\Delta t_{n-1})$], as shown in Sec. IV C. The existence of a significant correlation between q_n and Δt_n , can result in a $p_0(\Delta t_n)$, given by Eq. (13), that may deviate in behavior from that implied by Eqs. (36) and (37).

The tendency for the $p_0(q_n)$ distributions to approach a limiting narrow profile peaked at the high end for decreasing I_i as seen in Fig. 5 indicates that for any given set of discharge-gap conditions, there is a maximum mean amplitude q_{lim} that cannot be exceeded. This limit undoubtedly corresponds to the condition where the gap is largely free of residuals from previous pulses. Pulses for which $q_n \approx q_{lim}$ must therefore correspond to the "first-pulse" condition ($n = 1$) considered by Morrow.^{18,19} Figure 7 shows results for $p_0(q_n)$ using $N_2 + 20\% O_2$ for which the uv intensity was kept very low so that $(\Delta t_n) > 500 \mu s$. The gap conditions were similar to those used to obtain

the data for Figs. 3–5. As expected, q_{lim} increases with increasing V_a .

The widths of the distributions $p_0(q_n)$ as $q_{n,max} \rightarrow q_{lim}$ will be limited by inherent statistical fluctuations in discharge growth and gap conditions, e.g., statistical variations in the exact position on the cathode surface from which the initiating electron is released. For relatively small pulses below about 50 pC, noise in the pulse-detection circuit can limit the observable width of the pulse-height distribution. This limitation was not encountered for any of the data presented here.

The negative-corona pulses reported by Van Brunt and Leep⁷ in SF_6 that were found to be narrowly distributed in amplitude but widely distributed in time are undoubtedly Trichel pulses that satisfy the first-pulse condition. Similar pulses have recently been seen in SF_6-O_2 gas mixtures.²⁹

B. Behavior of $p_1(q_n|\Delta t_{n-1})$ and the $(q_n, \Delta t_{n-1})$ correlation

The interpretation of data for $p_0(q_n)$ and $p_0(\Delta t_n)$ given in Sec. IV A suggests that these distributions are not independent and that there must be a significant correlation between the random variables q_n and Δt_{n-1} . This correlation was verified by measuring $p_1(q_n|\Delta t_{n-1})$ at different Δt_{n-1} . Examples of data on $p_1(q_n|\Delta t_{n-1})$ for $N_2 + 20\% O_2$ are shown in Figs. 8 and 9, respectively, for high and low levels of uv irradiation. The discharge-gap

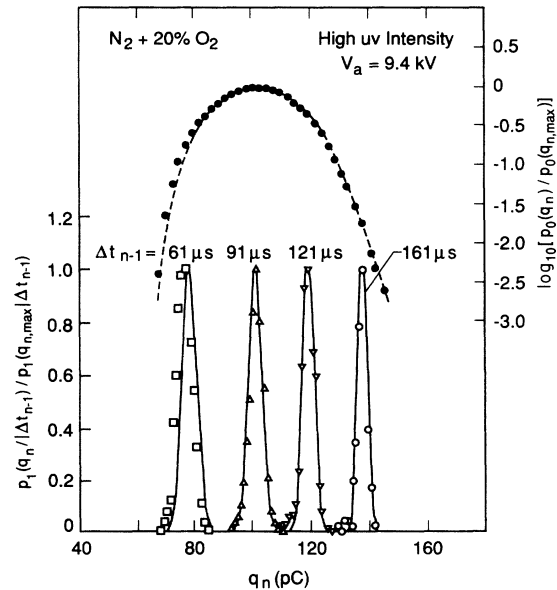


FIG. 8. Measured unconditional $p_0(q_n)$ and corresponding conditional $p_1(q_n|\Delta t_{n-1})$ distributions at 9.4 kV for the indicated values of Δt_{n-1} which apply to relatively intense uv irradiation of the cathode in a 100-kPa $N_2 + 20\% O_2$ gas mixture. The distributions have been normalized to the maximum values. The solid lines are Gaussian representations of the p_1 data which were used together with corresponding data on $p_0(\Delta t_n)$ in Eq. (10) to give the predicted $p_0(q_n)$ distribution indicated by the dashed line.

conditions used to obtain the results shown in Figs. 8 and 9 are similar to those that apply to Figs. 3-7.

The inequality $p_1(q_n|\Delta t_{n-1}) \neq p_0(q_n)$ seen from the data for allowed Δt_{n-1} implies a dependence of q_n on Δt_{n-1} . The dependence is positive, i.e., $\Delta t_{n-1} \uparrow \Rightarrow q_n \uparrow$. Because the widths of the $p_1(q_n|\Delta t_{n-1})$ are considerably narrower than the width of the corresponding unconditional distribution $p_0(q_n)$, the strong dependency condition defined in Sec. II B applies over at least a part of the range of allowed Δt_{n-1} . The strong $(q_n, \Delta t_{n-1})$ dependence was previously noted by Steiner²⁵ and is indicated here by the computed correlation coefficients $R_{q_n, \Delta t_{n-1}}$ shown in Fig. 10 for the case of high uv irradiation where $R_{q_n, \Delta t_{n-1}} \rightarrow 1$. At low uv intensity, $R_{q_n, \Delta t_{n-1}} \rightarrow 0$ as V_a decreases due to increasing contributions from time separations above Δt_ℓ (see Figs. 11 and 12) at which $p_1(q_n|\Delta t_{n-1})$ ceases to depend upon Δt_{n-1} , i.e., where $M_1(\Delta t_\ell, \Delta t_{n-1}) = 0$ for all $\Delta t_{n-1} > \Delta t_\ell$.

The interdependence of $p_0(q_n)$ and $p_0(\Delta t_n)$ was verified by using the measured $p_1(q_n|\Delta t_{n-1})$ distributions together with the measured $p_0(\Delta t_n)$ in Eq. (10) to compute $p_0(q_n)$. The results of these calculations, indicated by

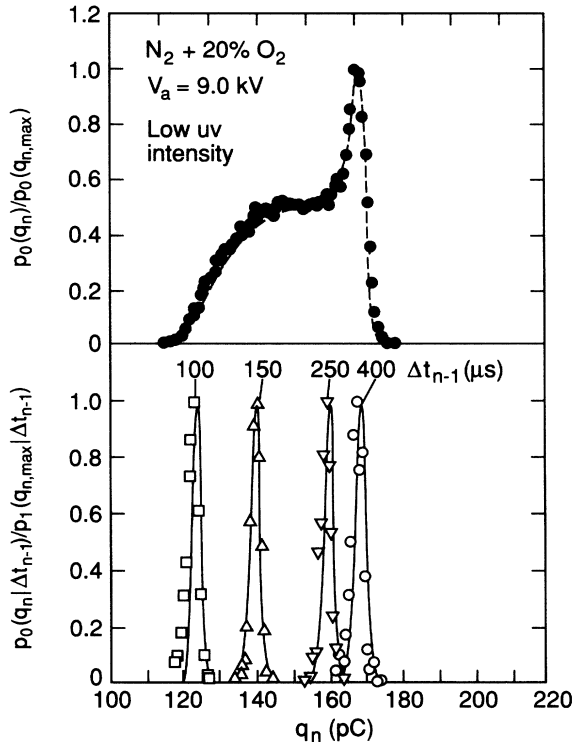


FIG. 9. Measured unconditional $p_0(q_n)$ and corresponding conditional $p_1(q_n|\Delta t_{n-1})$ distributions at 9.0 kV for the indicated values of Δt_{n-1} which apply to relatively weak uv irradiation of the cathode in a 100-kPa $N_2 + 20\% O_2$ gas mixture. The distributions have been normalized to the maximum values. The solid lines are Gaussian representations of the p_1 data which were used together with corresponding data on $p_0(\Delta t_n)$ in Eq. (10) to give the predicted $p_0(q_n)$ distribution indicated by the dashed line.

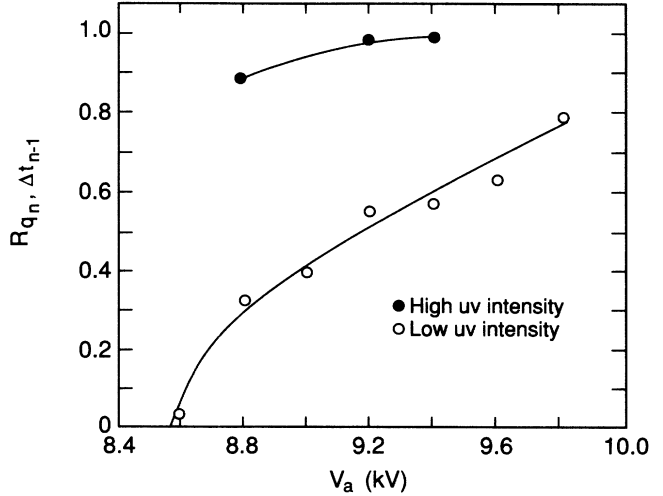


FIG. 10. Computed correlation coefficients for the random variables q_n and Δt_{n-1} as functions of discharge gap voltage (V_a) at two different indicated levels of relative uv intensity. Data for the measured $p_0(\Delta t_n)$, $p_0(q_n)$, and $p_1(q_n|\Delta t_{n-1})$ distributions similar to those shown in Figs. 8 and 9 were used in Eq. (4) to compute $R_{q_n, \Delta t_{n-1}}$.

the dashed lines in Figs. 8 and 9, are seen to agree satisfactorily with the measured $p_0(q_n)$, thereby demonstrating that the measured distributions are self-consistent and the profile of $p_0(q_n)$ is determined by the profile of $p_0(\Delta t_n)$ and the dependence of q_n on Δt_{n-1} .

When computing the integral in Eq. (10), Gaussian representations of the p_1 distributions shown in Figs. 9 and 10 were used as indicated by the solid lines. However, as shown by data for $Ne+5\% O_2$ given in Sec. IV D, the $p_1(q_n|\Delta t_{n-1})$ are generally non-Gaussian. In the case of $Ne+5\% O_2$, the measured $p_1(q_n|\Delta t_{n-1})$ can often be satisfactorily represented by the sum of two Gaussians given by

$$p_1(q_n|\Delta t_{n-1}) = \left[(2\pi)^{1/2} (\sigma_1 + c\sigma_2) \right]^{-1} \times \left\{ \exp \left[- (q_n - Q_1)^2 / 2\sigma_1^2 \right] + c \exp \left[- (q_n - Q_2)^2 / 2\sigma_2^2 \right] \right\}, \quad (38)$$

where c , σ_i , and Q_i ($i = 1, 2$) are dependent on Δt_{n-1} and obtained from fits to the data. An example of the Δt_{n-1} dependences of the Q_i parameters is shown in Fig. 11 for results from a $Ne+5\% O_2$ gas mixture together with corresponding data on $p_0(q_n)$ and $p_0(\Delta t_n)$. The result of evaluating the integral in Eq. (10) using the $p_0(\Delta t_n)$ shown in Fig. 11 and the above representation of $p_1(q_n|\Delta t_{n-1})$ are indicated by the dashed line and seen to be in satisfactory agreement with the measured $p_0(q_n)$. Indicated in this figure is the critical time Δt_ℓ above which the parameters in Eq. (38) cease to depend on Δt_{n-1} and $Q_1 = Q_2$ so that $p_1(q_n|\Delta t_{n-1})$ becomes adequately represented by a single Gaussian which is in-

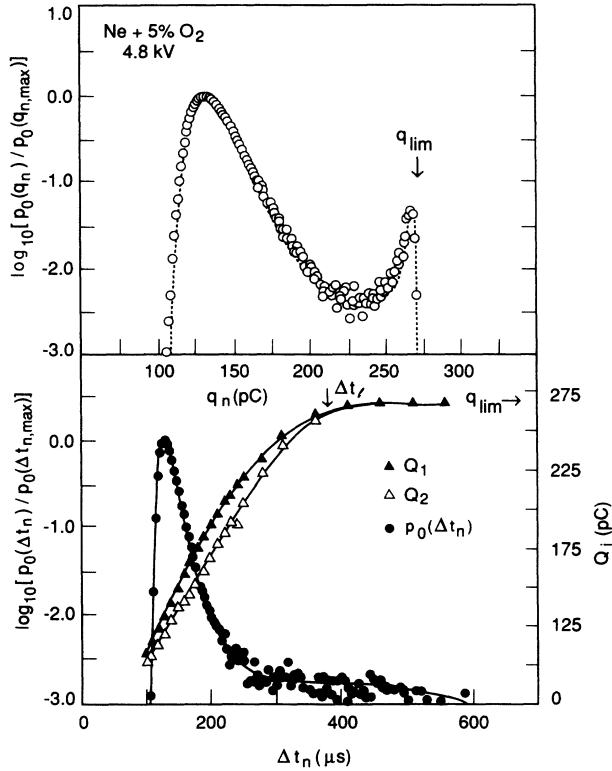


FIG. 11. Measured unconditional pulse-amplitude $p_0(q_n)$ and corresponding pulse-time-separation $p_0(\Delta t_n)$ distributions at 4.8 kV for relatively weak uv irradiation of the cathode in a 100-kPa Ne+5% O₂ gas mixture. Also shown are the Δt_n dependencies of the Q_i 's used in the double-Gaussian representation of the corresponding measured $p_1(q_n|\Delta t_{n-1})$ distributions as given by Eq. (38) with the indicated Q_i 's. The values for q_{lim} and Δt_l are marked with vertical arrows, and the dashed line represents $p_0(q_n)$ predicted from Eq. (10).

dependent of Δt_{n-1} .

The dependence of q_n on Δt_{n-1} implied by $p_1(q_n|\Delta t_{n-1})$ is that expected from the influence of the moving negative-ion space charge in the electrode gap as proposed independently by Lama and Gallo⁶ and Bugge.⁸ It is shown by these authors that several negative-ion space-charge clouds from previous discharge pulses can be present in the gap at the time a discharge pulse develops (see Fig. 14 of Ref. 6). The effect of negative-ion clouds anywhere in the gap is to reduce the electric-field magnitude at the cathode below the value it would have in the absence of such a cloud. This field reduction inhibits the growth of a discharge pulse. The greater the distance of the space-charge cloud from the cathode, the greater will be the field at the cathode and consequently the larger will be the magnitude of a discharge that develops at that time. As time elapses after the most recent discharge event, the space charge moves further from the point cathode thereby increasing the field in which the next pulse develops. The positive dependence of q_n on Δt_{n-1} can therefore be expected to hold until the critical time Δt_l is reached at which all the ions have arrived at

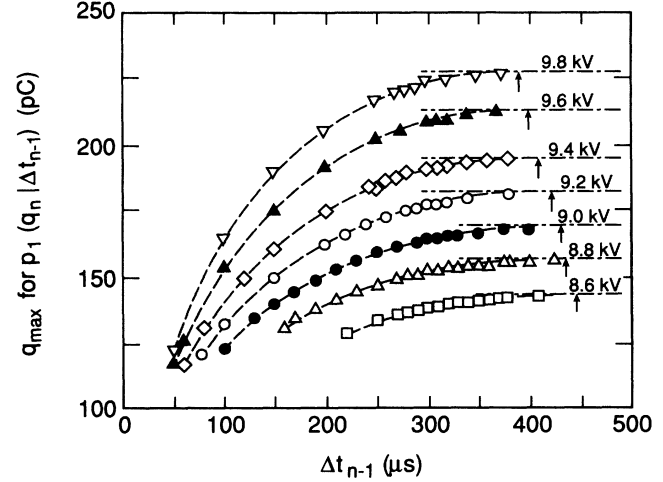


FIG. 12. Plot of $q_{max} \approx \langle q_n(\Delta t_{n-1}) \rangle$ vs Δt_{n-1} from $p_1(q_n|\Delta t_{n-1})$ data at the indicated applied gap voltages in the case of 100-kPa N₂ + 20% O₂ gas mixture. The vertical arrows correspond to Δt_l values estimated using Eqs. (40) and (41).

the anode. For $\Delta t_{n-1} > \Delta t_l$, the field at the cathode is restored to its unperturbed value and $q_n \rightarrow q_{lim}$.

The time Δt_l can be estimated using^{6,8}

$$\Delta t_l \approx \frac{1}{\mu} \int_0^{z_d} dz [E(z)]^{-1}, \quad (39)$$

where μ is the negative-ion mobility, z_d is the point-to-plane gap spacing, and $E(z)$ is the magnitude of the electric field on the point-to-plane axis for distance z measured from the cathode. A reasonable estimate⁶ for $E(z)$ is given by

$$E(z) \approx \frac{2V_a z_d}{\ln(4z_d/r_c)} g(z), \quad (40)$$

$$g(z) = [z_d(2z + r_c) - z^2]^{-1}, \quad (41)$$

where r_c is the cathode tip radius. This estimate neglects the ion space-charge distortion of the field, since it has been shown⁶ that this distortion has a minor effect on ion-drift times under conditions similar to those considered here.

Figure 12 shows plots of $q_{n,max} [\approx \langle q_n(\Delta t_{n-1}) \rangle]$ for $p_1(q_n|\Delta t_{n-1})$ versus Δt_{n-1} for different V_a and for a N₂ + 20% O₂ mixture with gap conditions like those used to obtain the data shown in Fig. 4. The dash-dotted lines correspond to the values for q_{lim} and the vertical arrows correspond to computed Δt_l values obtained from Eqs. (39)–(41) for the appropriate gap geometry and assuming a reasonable^{6,40} value for μ of 2.7 cm²/Vs. The computed Δt_l are seen to correspond approximately to the Δt_{n-1} values at which the $q_{n,max}$ versus Δt_{n-1} curves in Fig. 12 level off toward q_{lim} . This is also consistent with the behavior of $p_1(q_n|\Delta t_{n-1})$ implied by the data in Fig. 11 for Ne+5% O₂. The Δt_l values agree with

the ion transit times estimated for smaller gaps in air by Lama and Gallo.⁶ The implied dependence of Δt_ℓ on z_d was evident from measurements made in air using gap spacings from 0.2 to 10.0 cm. However, due to the waning influence of ion space charge with increasing distance from the cathode, Δt_ℓ becomes less clearly defined as z_d increases.

The strong dependence of q_n on Δt_{n-1} results from the sensitivity of discharge pulse growth to small changes in the electric field near the cathode. This sensitivity, as noted by Lama and Gallo,⁶ is due to the exponential dependence on field of the ionization processes that control discharge growth (also see Sec. IV E). The strong positive dependence of q_n on Δt_{n-1} appears to be a general characteristic of the Trichel-pulse phenomenon that applies over a wide range of conditions.²⁸⁻³⁰

C. Behavior of $p_1(\Delta t_n|q_n)$ and $p_1(\Delta t_n|\Delta t_{n-1})$

The $p_0(\Delta t_n)$ data for Ne+5% O₂ shown in Fig. 11 exhibit a behavior for $\Delta t_n > \Delta t_{n,\max}$ that is not consistent with Eq. (36). This suggests that the initiation of a discharge pulse is influenced not only by photoelectron emission via uv irradiation of the cathode but also

by self-excitation or retardation processes whereby residuals from earlier pulses serve to either enhance or inhibit the rate of electron release at the cathode. The extent to which self-excitation or retardation processes contribute is revealed from measured conditional time-separation distributions $p_1(\Delta t_n|q_n)$ and $p_1(\Delta t_n|\Delta t_{n-1})$.

Shown in Figs. 13 and 14 are data from $p_1(\Delta t_n|q_n)$ and $p_1(\Delta t_n|\Delta t_{n-1})$ measurements, respectively, in Ne+5% O₂ and N₂ + 20% O₂ gas mixtures for a relatively high level of uv irradiation comparable to that for the I₁ case shown in Fig. 5. The conditional distributions are compared with the corresponding unconditional distributions $p_0(\Delta t_n)$ indicated by the dashed lines in both figures. Correlations between the pairs $(\Delta t_n, q_n)$ and $(\Delta t_n, \Delta t_{n-1})$ for both mixtures are indicated by the lack of equality between the conditional and unconditional distributions. The correlations are strongest in the case of Ne+5% O₂ for which the dependence of Δt_n on q_n is positive, i.e., $q_n \uparrow \Rightarrow \Delta t_n \uparrow$. Consistent with this behavior, it is seen that $\Delta t_{n-1} \uparrow \Rightarrow \Delta t_n \uparrow$ as required by the arguments in Sec. II D. The signs of these dependences for the N₂ + 20% O₂ mixture are opposite to those for the Ne+5% O₂ mixture, i.e., $q_n \uparrow \Rightarrow \Delta t_n \downarrow$ and $\Delta t_{n-1} \uparrow \Rightarrow \Delta t_n \downarrow$. In both cases, the arguments

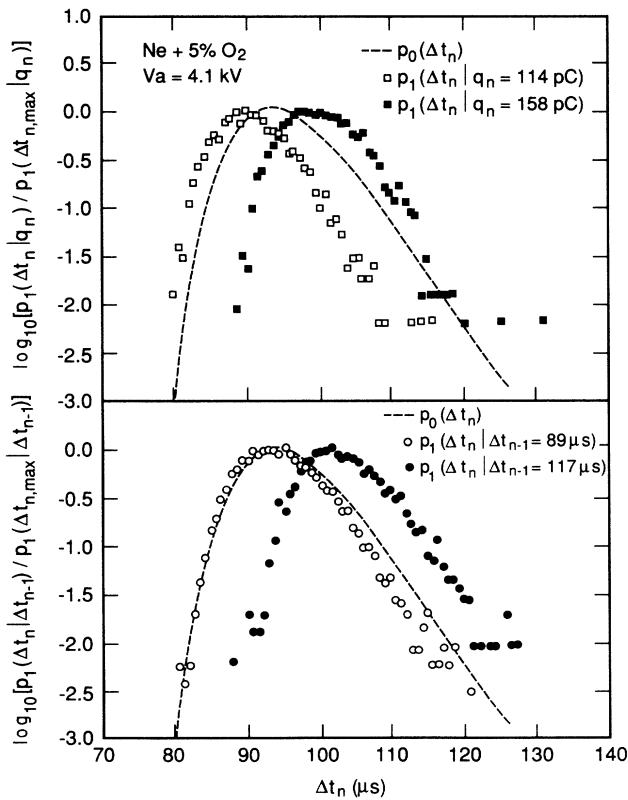


FIG. 13. Unconditional $[p_0(\Delta t_n)]$ and conditional $[p_1(\Delta t_n|\Delta t_{n-1})$ and $p_1(\Delta t_n|q_n)]$ time-separation distributions at the indicated Δt_{n-1} and q_n values for a 100-kPa Ne+5% O₂ mixture ($V_a = 4.1$ kV). The distributions have been normalized to the maxima.

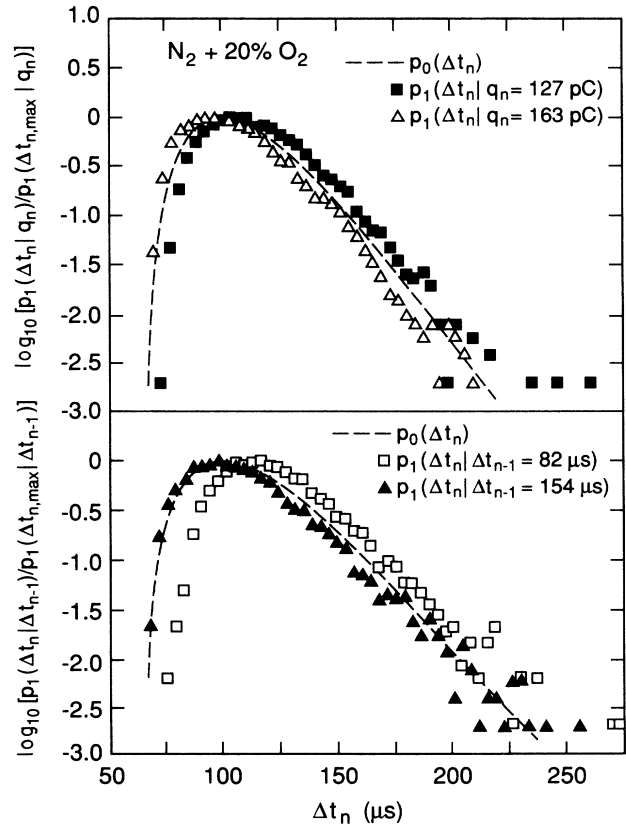


FIG. 14. Unconditional $[p_0(\Delta t_n)]$ and conditional $[p_1(\Delta t_n|\Delta t_{n-1})$ and $p_1(\Delta t_n|q_n)]$ time-separation distributions at the indicated Δt_{n-1} and q_n values for a 100-kPa N₂ + 20% O₂ mixture ($V_a = 9.1$ kV). The distributions have been normalized to the maxima.

in Sec. IID hold because the relatively high level of uv irradiation ensures that there is the required strong positive dependence of q_n on Δt_{n-1} over the entire range of time separations defined by $p_0(\Delta t_n)$ (see Fig. 10). Nevertheless, as shown by data in Sec. IVD, the relatively strong positive dependences between the pairs $(\Delta t_n, q_n)$ and $(\Delta t_n, \Delta t_{n-1})$ can persist even for weaker uv irradiation. A negative dependence of Δt_n on Δt_{n-1} was previously reported by Mason and Young³⁵ for negative-corona pulses in air which is comparable to the N_2 - O_2 case considered here.

One can only speculate at this time about the mechanisms responsible for the two different types of correlations implied by the results shown in Figs. 13 and 14. A careful investigation into the particular gap conditions that affect the observed behaviors of $p_1(\Delta t_n|q_n)$ and $p_1(\Delta t_n|\Delta t_{n-1})$ has not yet been undertaken. Measurements performed for varying $[Ne]/[O_2]$ ratios appear to indicate that the transition from positive to negative dependences occurs as the relative O_2 content in the gas increases. In Ne+95% O_2 and pure O_2 , the behavior is more like that found for the $N_2 + 20\% O_2$ case. Thus, although it appears that gas composition is relevant, it should be noted that in order to sustain the discharge, it is necessary to increase the electrode-gap voltage V_a as the O_2 content increases. This corresponding increase in V_a suggests that the electric-field intensity at the cathode may also be a relevant factor.

The behavior found for the Ne+5% O_2 case is that expected if the presence of ion space charge from the previous pulse acts to suppress the release of electrons from the cathode. This expectation is reasonable if electron release is primarily due to a field-assisted photoelectric effect³⁸ so that reductions in the field at the cathode by moving space charge serve to inhibit electron emission. An increase in q_n corresponds necessarily to an increase in the local negative-ion space-charge density, which in turn reduces the rate of electron release and correspondingly the probability for initiating the next pulse. The behavior of $p_1(\Delta t_n|q_n)$ indicated in Fig. 13 suggests that negative-ion space charge may reduce the cathode field enough to nearly turn off the electron release process for a significant interval of time following a "large" pulse.

The negative dependence of Δt_n on q_n found for $N_2 + 20\% O_2$ indicates that the probability for initiating a discharge pulse increases as the size of the previous pulse increases. This is possible if residual positive ions or metastable species from the previous pulse contribute to the release of initiatory electrons from the cathode. Because of the relatively long minimum times between pulses (greater than 50 μs), it is likely that metastable states have a more significant effect since positive-ion clearing times near the cathode should be comparable to Δt_c as noted by Lama and Gallo⁶ and Bugge.⁸

It was not possible to identify the role of specific metastable states that could yield initiatory electrons when quenched at the cathode surface. The $a^1\Delta_g$ and $b^1\Sigma_g^+$ metastable states of O_2 can be produced in the

discharge and are not readily quenched by collisions with either nitrogen or oxygen molecules.⁴¹⁻⁴⁴ The $A^3\Sigma_u^+$ state of N_2 has a long radiative lifetime (1-2 s), but is more readily quenched^{45,46} by collisions than the O_2 metastable states and may therefore have relatively less influence on secondary-electron release at the cathode under conditions of high gas pressure considered here. Its contribution to secondary-electron release has, nevertheless, been observed in low-pressure discharges.^{47,48} In the Ne- O_2 mixtures, the role of neon metastable states should also be considered, although the rates for collisional quenching of these metastable states in O_2 appear to be about two orders of magnitude higher than the rate for quenching the nitrogen $A^3\Sigma_u^+$ state.⁴⁹

For quenching of the O_2 $a^1\Delta_g$ state to be a source of secondary electrons at the cathode, a sufficiently intense electric field must be present to reduce the effective work function⁴⁰ of the stainless steel by at least 3 eV below that which it would have in the absence of a field.^{50,51} This might explain why the negative dependence of Δt_n on q_n appears for mixtures with relatively high O_2 concentrations for which higher voltages are needed to sustain the discharge. If field strengths are high enough for a field-assisted photoelectric effect, then field-assisted electron ejection by quenching of metastable states at the cathode surface would appear to be energetically possible. However, direct experimental confirmation of such a quenching process has yet to be reported. The presence of a high field could also influence the quenching of other more energetic metastable states such as the 1S and 1D metastable states of atomic oxygen. It was found that even for the Ne+5% O_2 mixture, the sign of the $(\Delta t_n, q_n)$ dependence becomes negative at higher V_a at which the discharge is largely self-sustained.

It should be noted that the space-charge effect that gives a positive dependence of Δt_n on q_n is operative independent of whether or not metastable states contribute to discharge-pulse initiation. When the negative $(\Delta t_n, q_n)$ dependence occurs, the effect of the metastables evidently overcomes that of space charge.

D. Behavior of $p_2(q_n|\Delta t_{n-1}, q_{n-1})$ and $p_2(q_n|\Delta t_{n-1}, \Delta t_{n-2})$

From the results presented here on $p_2(q_n|\Delta t_{n-1}, q_{n-1})$ and $p_2(q_n|\Delta t_{n-1}, \Delta t_{n-2})$, it will be seen that relatively strong dependences of q_n on q_{n-1} and on Δt_{n-2} are possible for fixed Δt_{n-1} which depend on the gas mixture used. Examples of data for the distributions $p_0(q_n)$, $p_1(q_n|\Delta t_{n-1})$, and $p_2(q_n|\Delta t_{n-1}, q_{n-1})$ obtained under the same conditions for a Ne+5% O_2 gas mixture are shown in Fig. 15. The gap conditions are similar to those that apply for the results shown in Fig. 11.

It is seen from these data that $p_2(q_n|\Delta t_{n-1}, q_{n-1}) \neq p_1(q_n|\Delta t_{n-1})$, and the expectation value $\langle q_n(q_{n-1}, \Delta t_{n-1}) \rangle$, given by

$$\langle q_n(q_{n-1}, \Delta t_{n-1}) \rangle = \int_0^\infty q_n p_2(q_n|\Delta t_{n-1}, q_{n-1}) dq_n, \quad (42)$$

increases for decreasing q_{n-1} at the indicated fixed values for Δt_{n-1} of 177, 197, and 217 μs . Since the widths of the p_2 distributions are much smaller than the widths of the corresponding p_1 distributions, it can be argued that there is a strong dependence of q_n on q_{n-1} which applies at these Δt_{n-1} values. Evidence for a negative (q_n, q_{n-1}) dependence was seen previously in the work of Cross and co-workers for Trichel pulses in low-pressure O_2 (see Fig. 12 of Ref. 13).

The dash-dotted lines in Fig. 15 represent Gaussian fits to the p_2 distributions which were used together with the data shown for $p_0(q_n)$ and a parametrized form for $p_1(\Delta t_n|q_n)$ in Eq. (14) to obtain computed $p_1(q_n|\Delta t_{n-1})$ indicated by the dashed lines. Under the conditions that apply for the data in Fig. 15, it was found that, in the approximate range $150 \mu\text{s} \lesssim \Delta t_{n-1} \lesssim 300 \mu\text{s}$, $p_1(\Delta t_{n-1}|q_{n-1})$ takes the form

$$p_1(\Delta t_{n-1}|q_{n-1}) = A_q \exp \left[-\omega_q (q_{n-1} - \beta_q)^2 \right], \quad (43)$$

where ω_q and β_q are constants that satisfy the requirements $\omega_q > 0$ and $\beta_q \gtrsim q_{\text{lim}}$. The constant A_q is necessary for proper normalization, but becomes irrelevant in Eq. (14) if $p_1(q_n|\Delta t_{n-1})$ is normalized to the maximum value as in Fig. 15. The factor $p_0(\Delta t_{n-1})^{-1}$ in Eq. (14) is also irrelevant for the same reason. The values for ω_q and β_q that were used to obtain the dashed lines in Fig. 15

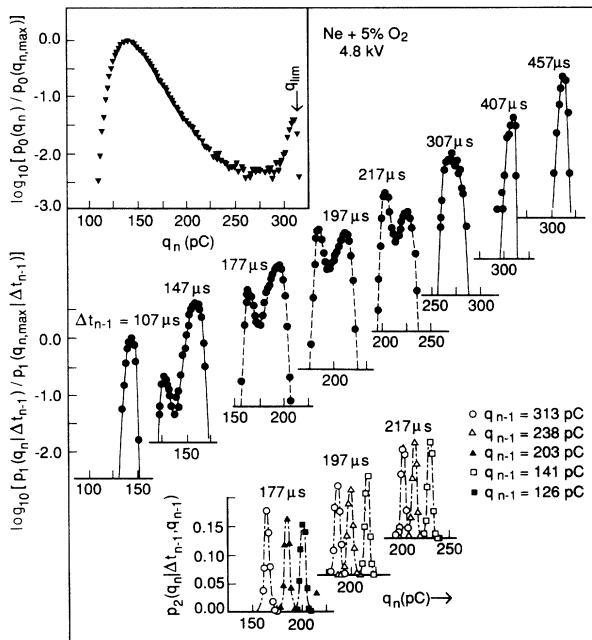


FIG. 15. Measured $p_0(q_n)$, $p_1(q_n|\Delta t_{n-1})$, and $p_2(q_n|\Delta t_{n-1})$ distributions for the indicated values for Δt_{n-1} and q_{n-1} at $V_a = 4.8 \text{ kV}$ in a 100-kPa $\text{Ne} + 5\% \text{O}_2$ mixture. The dash-dotted lines are Gaussian representations of the p_2 data used together with the $p_0(q_n)$ data and $p_1(\Delta t_{n-1}|q_{n-1})$ given by Eq. (43) (also see Table II) in Eq. (14) to obtain the predicted $p_1(q_n|\Delta t_{n-1})$ indicated by the dashed lines at 177, 197, and 217 μs .

TABLE II. Parameter values for $p_1(\Delta t_{n-1}|q_{n-1})$ [Eq. (43)] used in Eq. (14) to obtain the dashed-line representations for $p_1(q_n|\Delta t_{n-1})$ in Fig. 15 at the indicated Δt_{n-1} values.

Δt_{n-1} (μs)	ω_q (pC^{-2})	β_q (pC)
177	0.823×10^{-4}	350
197	1.18×10^{-4}	336
217	1.22×10^{-4}	355

at the indicated time separations Δt_{n-1} are listed in Table II. In this case it is seen that the β_q are all slightly larger than the corresponding q_{lim} value of 320 pC given by the $p_0(q_n)$ data in Fig. 15.

The approximate form for $p_1(\Delta t_{n-1}|q_{n-1})$ given by Eq. (43) is consistent with experimentally observed trends, as indicated by data in Fig. 16, which apply to conditions similar but not identical to those for Fig. 15. For the conditions that apply to Fig. 16, it is evident that Eq. (43) becomes a reasonable representation for $p_1(\Delta t_{n-1}|q_{n-1})$ when Δt_{n-1} is somewhat greater than 170 μs . In the Δt_{n-1} range 150–170 μs , $p_1(\Delta t_{n-1}|q_{n-1})$ shows much less variation with q_{n-1} than implied by Eq. (43), and for sufficiently low Δt_{n-1} , $p_1(\Delta t_{n-1}|q_{n-1})$

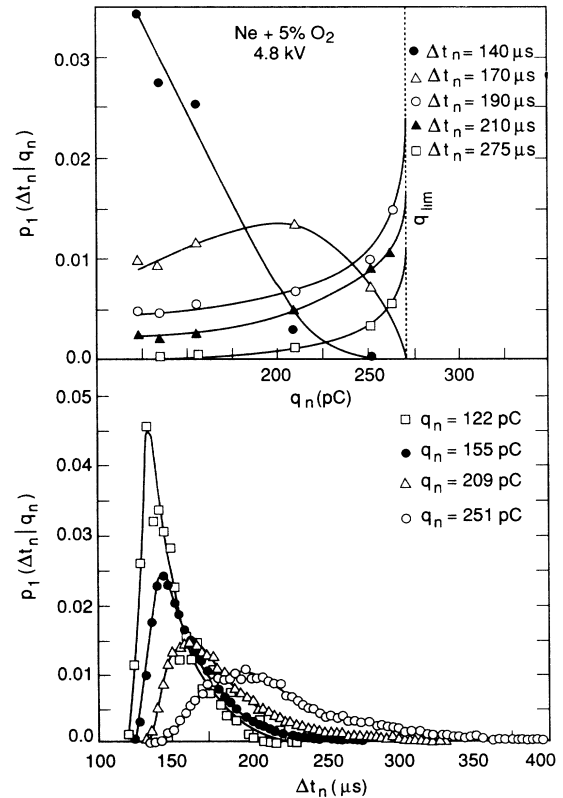


FIG. 16. Conditional time-separation distribution $p_1(\Delta t_n|q_n)$ plotted vs q_n for the indicated Δt_{n-1} values (top) and vs Δt_n for the indicated q_n values (bottom) for conditions similar to those that apply to Fig. 15.

decreases rapidly with q_{n-1} as indicated by the $140\ \mu\text{s}$ curve in Fig. 16. The general trends implied by the data in this figure apply over a wide range of conditions. It should be noted that the variations in the shapes of the $p_1(q_n|\Delta t_{n-1})$ distributions with Δt_{n-1} can be accounted for by the variations in the behavior of $p_1(\Delta t_{n-1}|q_{n-1})$ implied by the results in Fig. 16. If $p_1(\Delta t_{n-1}|q_{n-1})$ is assumed to be constant (independent of q_{n-1}) as is approximately true for Δt_{n-1} in a narrow range around $150\ \mu\text{s}$, then the $p_1(q_n|\Delta t_{n-1})$ assume shapes similar to that indicated by the $147\ \mu\text{s}$ data in Fig. 15. In this case the shape is a compressed, inverse reflection of the $p_0(q_n)$ distribution due to the negative (q_n, q_{n-1}) dependence. Thus variations in the $p_1(q_n|\Delta t_{n-1})$ profile of the type seen here imply a significant dependence of Δt_n on q_n .

Figure 17 shows results for the $p_0(\Delta t_n)$, $p_1(q_n|\Delta t_{n-1})$, and $p_2(q_n|\Delta t_{n-1}, \Delta t_{n-2})$ distributions obtained for a condition similar to that which applies to the data in Fig. 15. From the data on p_2 it is seen that there is a negative dependence of q_n on Δt_{n-2} as required by the corresponding negative (q_n, q_{n-1}) dependence and the strong positive ($q_n, \Delta t_{n-1}$) dependence (see Sec. II E.). Moreover, the correlation between q_n and Δt_{n-2} at the indicated Δt_{n-1} values appears to satisfy the strong-dependency condition.

The dashed curves at 177, 197, and $217\ \mu\text{s}$ are the results of performing the integral of Eq. (18) in which Gaussian representations of the p_2 distributions shown

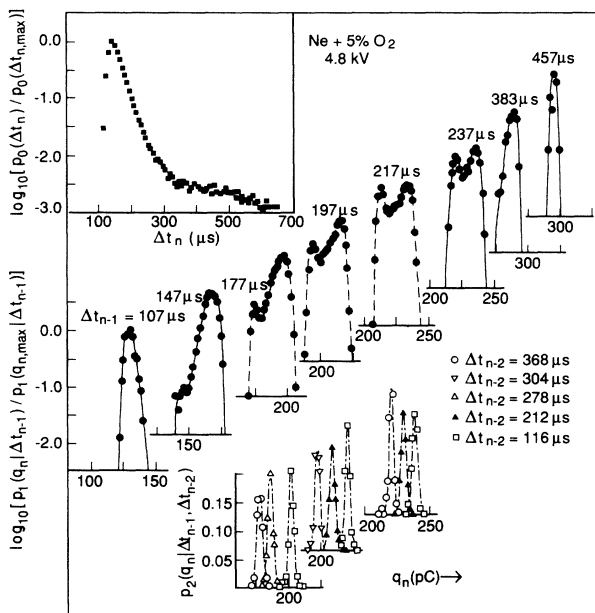


FIG. 17. Measured $p_0(\Delta t_n)$, $p_1(q_n|\Delta t_{n-1})$, and $p_2(q_n|\Delta t_{n-1}, \Delta t_{n-2})$ distributions for the indicated values of Δt_{n-1} and Δt_{n-2} at $V_a = 4.8\ \text{kV}$ in a 100-kPa $\text{Ne}+5\%\text{O}_2$ mixture. The dash-dotted lines on Gaussian representations of the p_2 data used together with the $p_0(\Delta t_n)$ data and $p_1(\Delta t_{n-1}|\Delta t_n)$ given by Eqs. (44) and (45) (also see Table III) in Eq. (18) to obtain the predicted $p_1(q_n|\Delta t_{n-1})$ indicated by the dashed lines at 177, 197, and $217\ \mu\text{s}$.

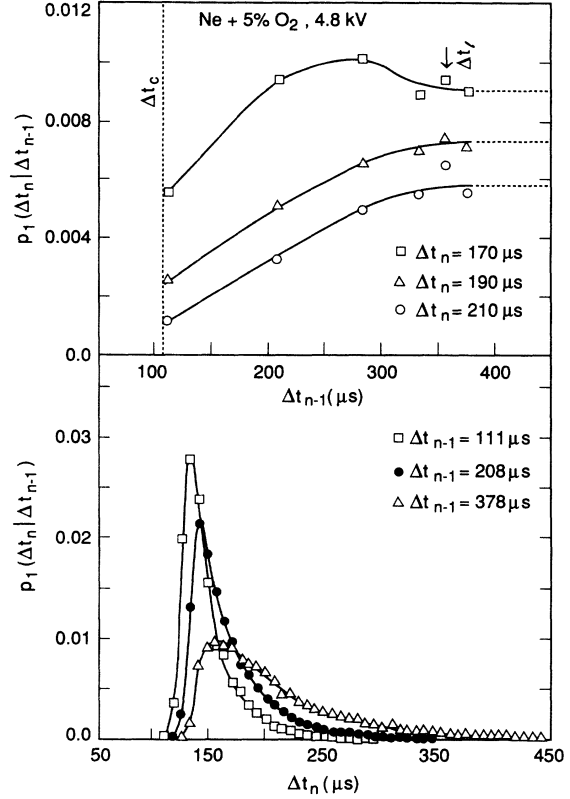


FIG. 18. Conditional time-separation distribution $p_1(\Delta t_n|\Delta t_{n-1})$ plotted vs Δt_{n-1} for the indicated Δt_n values (top) and vs Δt_n for the indicated Δt_{n-1} values (bottom) for conditions similar to those that apply to Fig. 16.

by the dash-dotted lines and the numerical data shown for $p_0(\Delta t_n)$ were used together with a parametrized form for $p_1(\Delta t_{n-1}|\Delta t_{n-2})$. In this case the conditional time-separation distribution was given the form

$$p_1(\Delta t_{n-1}|\Delta t_{n-2}) = A_t \exp \left[-\omega_t (\beta_t - \Delta t_{n-2})^2 \right] \quad (44)$$

for $\Delta t_{n-2} \leq \beta_t$, and

$$p_1(\Delta t_{n-1}|\Delta t_{n-2}) = A_t \quad (45)$$

for $\Delta t_{n-2} > \beta_t$.

This is the approximate form suggested by the $p_1(\Delta t_n|\Delta t_{n-1})$ data shown in Fig. 18. When Δt_{n-2} exceeds about $180\ \mu\text{s}$, the parameter β_t approaches the value of Δt_t , which for the data in Fig. 17 is about $410\ \mu\text{s}$. The values of the parameters used in Eq. (44) to obtain the calculated $p_1(q_n|\Delta t_{n-1})$ in Fig. 17 are given in Table III.

The observed negative dependence of q_n on q_{n-1} (and correspondingly of q_n on Δt_{n-2}) in the $\text{Ne}+5\%\text{O}_2$ gas mixture can be qualitatively accounted for by the effect of the negative-ion space charge from the previous discharge pulse on suppressing the growth of the subsequent pulse. In this case it is the size of the space-charge cloud

TABLE III. Parameter values for $p_1(\Delta t_{n-1}|\Delta t_{n-2})$ [Eqs. (44) and (45)] used in Eq. (18) to obtain the dashed-line representations for $p_1(q_n|\Delta t_{n-1})$ in Fig. 17 at the indicated Δt_{n-1} values.

Δt_{n-1} (μs)	ω_t (μs^{-2})	β_t (μs)
177	1.54×10^{-4}	280
197	0.503×10^{-4}	400
217	0.516×10^{-4}	422

rather than its location that is relevant. The larger the previous pulse, the larger its resulting negative-ion cloud and, consequently, the greater the reduction of the field at the cathode for any given $\Delta t_{n-1} < \Delta t_t$. This field reduction serves to inhibit the growth of the next pulse; thus larger pulses will preferentially be followed, on the average, by smaller pulses and vice versa.

It was observed that in some gas mixtures with higher O_2 content the dependence of q_n on q_{n-1} reverses sign and becomes positive. This was demonstrated by results published previously for the $\text{N}_2 + 20\% \text{O}_2$ mixture (see Fig. 7 of Ref. 27). Shown in Fig. 19 are examples of data on $p_2(q_n|\Delta t_{n-1}, q_{n-1})$ distributions for a $\text{Ne}+95\% \text{O}_2$ mixture at different indicated gap voltages that clearly indicate a positive (q_n, q_{n-1}) dependence for sufficiently small Δt_{n-1} . The positive dependences are weaker than the negative dependences found for $\text{Ne}+5\% \text{O}_2$ shown by the data in Fig. 15. The dependence of q_n on q_{n-1} begins to disappear for $\Delta t_{n-1} \gtrsim 75 \mu\text{s}$ where $p_2(q_n|\Delta t_{n-1}, q_{n-1})$ ceases to depend on q_{n-1} . In the case of $\text{N}_2 + 20\% \text{O}_2$ mixtures, the positive dependence of q_n on q_{n-1} was found²⁷ to persist even for Δt_{n-1} in excess of $100 \mu\text{s}$. It should be noted incidently from Fig. 19 that even the $p_2(q_n|\Delta t_{n-1}, q_{n-1})$ distributions may exhibit distinctly non-Gaussian shapes.

The appearance of a positive (q_n, q_{n-1}) dependence often coincides with a negative dependence of Δt_n on q_n as illustrated by the data in Fig. 14 for $\text{N}_2 + 20\% \text{O}_2$. It was suggested in Sec. IV C that the negative ($\Delta t_n, q_n$) dependence may be a manifestation of the influence of metastable species on electron release from the cathode. The occurrence of the positive (q_n, q_{n-1}) dependence suggests that the metastable densities produced by earlier discharge pulses are high enough to significantly increase the effective ionization coefficient of the gas in the immediate vicinity of the cathode at the time that the next pulse develops. An increase in the local ionization coefficient enhances discharge growth.

As shown by Van Brunt⁵² from an extension of Legler's⁵³ analysis, the probability that the initial electron avalanche consists of n_e electrons after growing a distance z from the cathode on the point-to-plane axis is given to a good approximation by

$$p_1(n_e|z) dz = \frac{1}{w(z)^2} \exp[u(z)] \exp[n_e/w(z)] dz, \quad (46)$$

where

$$u(z) \equiv \int_0^z [\alpha_i(z') - \eta_a(z')] dz' \quad (47)$$

and

$$w(z) \equiv 1 + \exp[u(z)] \int_0^z \alpha_i(z') \exp[-u(z')] dz'. \quad (48)$$

In Eqs. (46)–(48), α_i and η_a are, respectively, the ionization and attachment coefficients of the gas which depend on the electric-field-to-gas density ratio $E(z)/N$ and therefore on z . The middle term in Eq. (46) indicates an exponential dependence on $(\alpha_i - \eta_a)$. Thus even relatively small changes in α_i due to either changes in $E(z)$ or presence of metastables could have disproportionately large effects on the electron-avalanche growth in the ini-

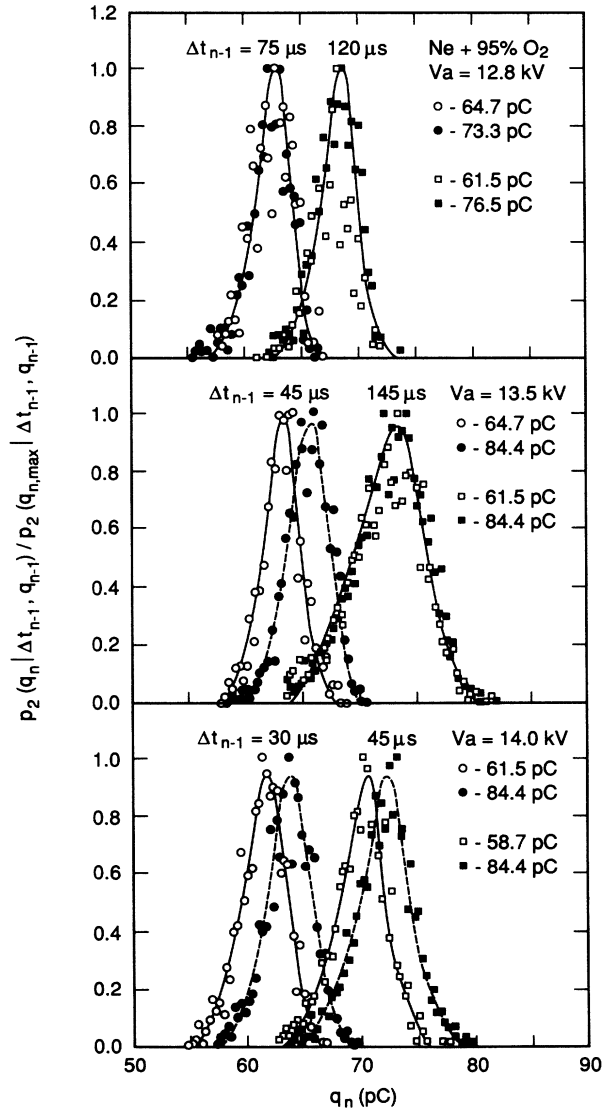


FIG. 19. Measured $p_2(q_n|\Delta t_{n-1}, q_{n-1})$ distributions at the indicated q_{n-1} and Δt_{n-1} values for different applied gap voltages in a 100-kPa $\text{Ne}+95\% \text{O}_2$ mixture. The distributions have been normalized to the maxima.

tial stages of Trichel-pulse formation. It is also this factor that comes into play in accounting for the strong dependence of q_n on Δt_{n-1} .

To determine the plausibility of the suggested influence of metastable species on local ionization-coefficient enhancement near the cathode, estimates were made of the resident times for metastable states in the active region of the cathode defined by the Geballe-Reeves breakdown criterion,⁵⁴ namely that region where $\alpha_i > \eta_a$. The spatial extent of this region for the case of unperturbed fields was estimated using Eqs. (40) and (41) and the recommended values⁵⁵ for α_i and η_a that apply to air and therefore to the $N_2 + 20\% O_2$ mixture. The active region was assumed to be approximately⁵² spherical of radius R_{crit} . The value for R_{crit} corresponds to $z_c/2$, where $E(z_c)$ is the axial field strength at which $\alpha_i = \eta_a$. Note that Eq. (46) requires that the initial electron-avalanche growth cease if $z > z_c$.

The rate equation for neutral metastable-species transport in the gas is⁵⁶

$$\frac{\partial \rho(\mathbf{r}, t)}{\partial t} = D \nabla^2 \rho(\mathbf{r}, t) - k_m N \rho(\mathbf{r}, t) - (1/\tau_m) \rho(\mathbf{r}, t). \quad (49)$$

$$\rho(r, t) = \frac{3/2 \rho_0 \exp(-k_m N t)}{(4\pi)^{3/2} (Dt)^{1/2} R_{crit}^3 r} \int_0^{R_{crit}} r' \left[\exp\left(\frac{-r^2 - r'^2 + 2rr'}{4Dt}\right) - \exp\left(\frac{-r^2 - r'^2 - 2rr'}{4Dt}\right) \right] dr'. \quad (51)$$

If the metastable species are to be effective in modifying α_i at the time of the next pulse, a significant fraction must remain in V_{crit} for $\Delta t_{n-1} > \Delta t_c$. The collisional-quenching rate must therefore satisfy the condition

$$k_m < (N \Delta t_c)^{-1}. \quad (52)$$

For Δt_c in the range 10–300 μs at atmospheric pressure (see Fig. 6), Eq. (52) requires that k_m lie above the corresponding values 4.0×10^{-15} to 1.4×10^{-16} cm^3/s . This condition is satisfied by the $a^1\Delta_g$ and $b^1\Sigma_g^+$ states of oxygen,^{41–44} but not by the metastable states of either nitrogen^{45,46} or neon.⁴⁹ In the case of the oxygen metastable states, $k_m \ll (N \Delta t_c)^{-1}$ and therefore $\exp(-k_m N t) \simeq 1$ in Eq. (51). This approximation may also apply to long-lived, vibrationally excited N_2 .

Results of computing $F(t)$ in the case where collisional quenching can be neglected are shown in Fig. 20. It is seen from this figure that, independent of the assumed value for D in the range 0.5×10^{-7} to 5.0×10^{-7} cm^2/s , a significant fraction of the metastable species is present in V_{crit} for times up to 100 μs after cessation of the discharge pulse. Thus it can be concluded that metastable species generated in a discharge pulse remain near the cathode for times long enough to influence development of the next pulse.

The extent to which metastable species influence discharge growth depends on ρ_0 , i.e., on the number produced in V_{crit} . It should be realized, however, that the

Here $\rho(\mathbf{r}, t)$ is the metastable density at position \mathbf{r} and time t , D is the metastable diffusion coefficient, k_m is the rate coefficient for collisional quenching, and τ_m is the radiative life time. Only metastable states for which $\tau_m > \Delta t_c$ are considered here; thus the last term on the right-hand side of Eq. (49) can be neglected. Assuming spherical symmetry, Eq. (49) can be solved to give the fraction $F(t)$ of metastable states remaining in the volume V_{crit} defined by $r \geq R_{crit}$ at a time t after cessation of a discharge pulse. Consistent with the experimental conditions, the diameter of the discharge vessel is assumed to be much larger than R_{crit} so that wall effects can be neglected.

If the discharge pulse leaves a uniformly distributed metastable density ρ_0 that is confined to V_{crit} , then it can be shown from the solution of Eq. (49) that

$$F(t) = \int_0^{R_{crit}} r^2 \rho(r, t) dr / \int_0^\infty r^2 \rho(r, t) dr, \quad (50)$$

where

effect of metastable species on the gas ionization coefficient can be disproportionately larger than implied by their relative densities. This is due to the fact that metastable species have a significantly lower ionization threshold than the corresponding neutral molecules in their ground state. The local ionization coefficient in the gas at any time t is given by^{57,58}

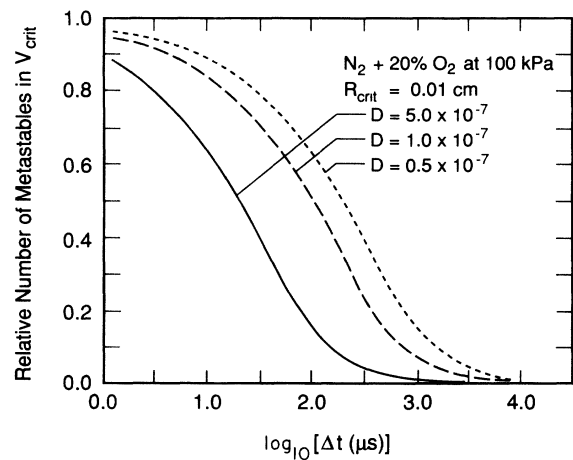


FIG. 20. Calculated fraction of metastable states remaining in the critical volume V_{crit} near the cathode at a time Δt following cessation of a discharge pulse for different assumed values of the diffusion coefficient.

$$\alpha_i(\mathbf{r}, t) = (2m_e)^{1/2} (NW_m)^{-1} \times \left(\sum_j \rho_j K_j + \sum_k \rho_k(\mathbf{r}, t) K_k \right), \quad (53)$$

where

$$K_\ell = \int_{\epsilon_\ell} \epsilon f_m(\mathbf{r}, t, \epsilon) \sigma_{I_\ell}(\epsilon) d\epsilon, \quad \ell = j \text{ or } k. \quad (54)$$

In Eqs. (53) and (54) m_e is the electron mass, $N (= \sum_\ell \rho_\ell)$ is the total particle density, W_m is the electron drift velocity, ρ_j is the local density of the j th neutral species in the ground state, ρ_k is the density of the k th metastable species, ϵ is the electron translational kinetic energy, ϵ_ℓ is the ionization threshold energy for the ℓ th species, $\sigma_{I_\ell}(\epsilon)$ is the electron-impact ionization cross section for the ℓ th species, and f_m is the kinetic-energy distribution of the electrons. In general, N , W_m , ρ_j , ρ_k , and f_m depend on \mathbf{r} and t . However, if $N \gg \rho_k$ for any k , then the dependence of α_i on t is primarily that due to $\rho_k(\mathbf{r}, t)$. The spatial dependence of α_i is governed by the field and the density distribution of the diffusing metastable species.

Because the ionization thresholds ϵ_ℓ typically have values that fall in the high-energy tail⁵⁷ of f_m at moderate E/N for which $\alpha_i > \eta_a$, it can be expected that K_ℓ will increase rapidly with decreasing ϵ_ℓ . Thus even relatively small metastable concentrations can be responsible for disproportionately large enhancements in α_i . The influence of low metastable concentrations on gas-ionization rates manifests itself in the well-known optogalvanic effect,⁵⁹ which has been observed in both neon⁶⁰ and nitrogen⁶¹ discharges at low pressures.

E. Behavior of $p_1(q_n|q_{n-1})$ and $p_1(q_n|\Delta t_{n-2})$, $j \geq 2$

If relatively strong dependences of q_n on Δt_{n-2} (or q_{n-1}) occur at a fixed value of Δt_{n-1} as implied by the data on $p_2(q_n|\Delta t_{n-1}, \Delta t_{n-2})$ and $p_2(q_n|\Delta t_{n-1}, q_{n-1})$, respectively, then it can be expected from Eqs. (20) and (15) that dependences of q_n on Δt_{n-2} (or q_{n-1}) will exist independent of Δt_{n-1} . The sign of the $(q_n, \Delta t_{n-2})$ dependence implied by Eq. (20) depends on the signs and relative strengths of the dependences between the pairs $(\Delta t_{n-1}, \Delta t_{n-2})$ and $(q_n, \Delta t_{n-2})$ for fixed Δt_{n-1} and should be the same as that for the (q_n, q_{n-1}) dependence.

Figure 21 shows examples of measured $p_1(q_n|\Delta t_{n-2})$ and $p_1(q_n|q_{n-1})$ distributions for different indicated values for Δt_{n-2} and q_{n-1} . The results are compared with the corresponding unconditional distributions $p_0(q_n)$, indicated by the solid lines. The expectation values $\langle q_n(\Delta t_{n-2}) \rangle$ and $\langle q_n(q_{n-1}) \rangle$ decrease with increasing Δt_{n-2} and q_{n-1} , respectively, thus giving negative dependences, i.e., $\Delta t_{n-2} \uparrow \Rightarrow q_n \downarrow$ and $q_{n-1} \uparrow \Rightarrow q_n \downarrow$. The measured $p_1(q_n|\Delta t_{n-2})$ distributions are consistent with the corresponding measured distributions $p_1(\Delta t_{n-1}|\Delta t_{n-2})$ and $p_2(q_n|\Delta t_{n-1}, \Delta t_{n-2})$

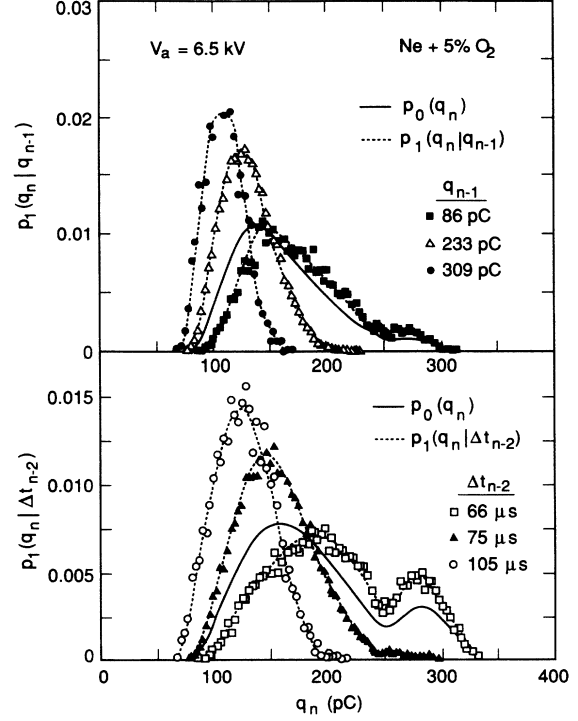


FIG. 21. Measured conditional pulse-amplitude distributions $p_1(q_n|\Delta t_{n-2})$ and $p_1(q_n|q_{n-1})$ at the indicated gap voltage and values for Δt_{n-2} and q_{n-1} in a 100-kPa Ne+5% O₂ gas mixture.

as determined by Eq. (20), which applies for a strong $(q_n, \Delta t_{n-1})$ dependence. Because of the relatively high value of V_a and low uv intensity, both the (q_n, q_{n-1}) and $(\Delta t_{n-1}, \Delta t_{n-2})$ dependences were negative. Therefore the effect of p_1 in this case was to reinforce the $(q_n, \Delta t_{n-2})$ correlation implied by p_2 in Eq. (20). Because of the strong $(q_{n-1}, \Delta t_{n-2})$ dependence, the measured $p_1(q_n|q_{n-1})$ distributions in Fig. 21 behave like the $p_1(q_n|\Delta t_{n-2})$ distributions and are consistent with Eq. (15) as discussed in Sec. II E.

The measured $p_1(q_n|\Delta t_{n-2})$ for the N₂ + 20% O₂ mixture^{27,30} did not generally deviate significantly from $p_0(q_n)$. This is probably due largely to the fact that, in this case, the observed dependence of q_n on Δt_{n-2} for fixed Δt_{n-1} was considerably weaker than in the Ne+5% O₂ case. Note that in the limit of very weak correlations where $p_2(q_n|\Delta t_{n-1}, \Delta t_{n-2}) \simeq p_1(q_n|\Delta t_{n-1})$ and $p_1(\Delta t_{n-1}|\Delta t_{n-2}) \simeq p_0(\Delta t_{n-1})$, Eq. (20) reduces to Eq. (10), which simply gives $p_0(q_n)$. Also, in the N₂ + 20% O₂ case, the signs of the $(q_n, \Delta t_{n-2})$ and $(\Delta t_{n-1}, \Delta t_{n-2})$ dependences implied, respectively, by p_1 and p_2 in Eq. (20) tend to counteract each other.

A comparison of results obtained for $p_1(q_n|\Delta t_{n-j})$, $j = 1, 2, 3, 4$, from a Ne+5% O₂ mixture is shown in Fig. 22 for two different gap voltages and three different values for Δt_{n-j} . These results represent fits to the numerical data that have been normalized to the maxima.

The lowest Δt_{n-j} values correspond to time separations closest to Δt_c in the $p_0(\Delta t_n)$ distributions, whereas the intermediate and largest values correspond, respectively, to the maxima and high ends of these distributions. The ratios of expectation values, $\langle q_n(\Delta t_{n-j}) \rangle / \langle q_n \rangle$, obtained from the corresponding distributions in Fig. 22, are shown graphically in Fig. 23. Here $\langle q_n \rangle$ corresponds to $p_0(q_n)$ as given by Eq. (33). The bars shown in Fig. 23 represent the approximate limits for statistically significant differences between $\langle q_n(\Delta t_{n-j}) \rangle$ and $\langle q_n \rangle$ and provide a measure of the extent to which the $p_1(q_n|\Delta t_{n-j})$ and $p_0(q_n)$ distributions differ.

The previously discussed positive ($q_n, \Delta t_{n-1}$) and negative ($q_n, \Delta t_{n-2}$) dependences are clearly demonstrated in Fig. 23. A statistically significant positive ($q_n, \Delta t_{n-3}$) dependence is evident from the 7.2-kV data. The 6.8-kV data suggest a nonmonotonic behavior in the ($q_n, \Delta t_{n-3}$) dependence. Nonmonotonic behavior in the sign of the ($q_n, \Delta t_{n-3}$) dependence occurs under some conditions. However, for the data shown in Fig. 23, it is of questionable statistical significance.

Except at the very lowest Δt_{n-4} values, the $p_1(q_n|\Delta t_{n-4})$ distributions did not differ significantly from the corresponding $p_0(q_n)$ distributions. The $p_1(q_n|\Delta t_{n-4})$ results generally exhibit the hint of a negative ($q_n, \Delta t_{n-4}$) dependence over at least the lower part of the Δt_{n-4} range. The lack of equality between $p_1(q_n|\Delta t_{n-j})$ and $p_0(q_n)$, which can occur even for $j = 4$, unequivocally shows that memory extends back considerably beyond the preceding event. This agrees with

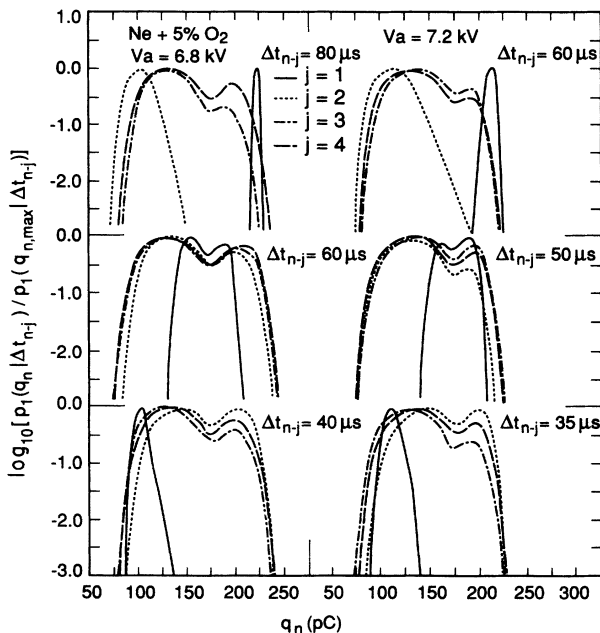


FIG. 22. Measured conditional pulse-amplitude distributions $p_1(q_n|\Delta t_{n-j})$ for the indicated j and Δt_{n-j} values for $V_a = 6.2$ and 7.2 kV in a 100-kPa Ne+5%O₂ gas mixture. The distributions have been normalized to the maximum values.

recent observations of Steiner²⁵ by a completely different method and conclusively demonstrates that Trichel-pulse corona is indeed a non-Markovian stochastic process. The alternating signs of the correlations with increasing j are consistent with the arguments in Sec. II F.

In the present experiment, only conditional pulse-amplitude distributions up to second order could be measured (see Table I). However, the data for $p_2(q_n|\Delta t_{n-1}, q_{n-1})$ and $p_2(q_n|\Delta t_{n-1}, \Delta t_{n-2})$ shown in Figs. 15 and 17, respectively, indicate that it would be difficult to observe correlations between q_n and either q_{n-2} or Δt_{n-3} even if p_3 distributions could have been measured. This is a consequence of inherent limitations in the instrumental resolution such as determined by amplifier noise and number of MCA channels. Thus, although memory may extend indefinitely back in time, there are instrumental limitations to assessing the extent of memory propagation for large values of j ($j \gtrsim 4$ in the present case). It is shown in the Appendix that, for the present experimental situation in which second-order correlations between q_n and Δt_{n-2} can easily be resolved, $j = 4$ is the lowest value of j for which the profiles of the $p_1(q_n|\Delta t_{n-j})$ and $p_0(q_n)$ distributions could become indistinguishable at all allowed values for Δt_{n-j} .

V. SUMMARY AND CONCLUSIONS

The experimental results presented here demonstrate unequivocally that the Trichel-pulse discharge phe-

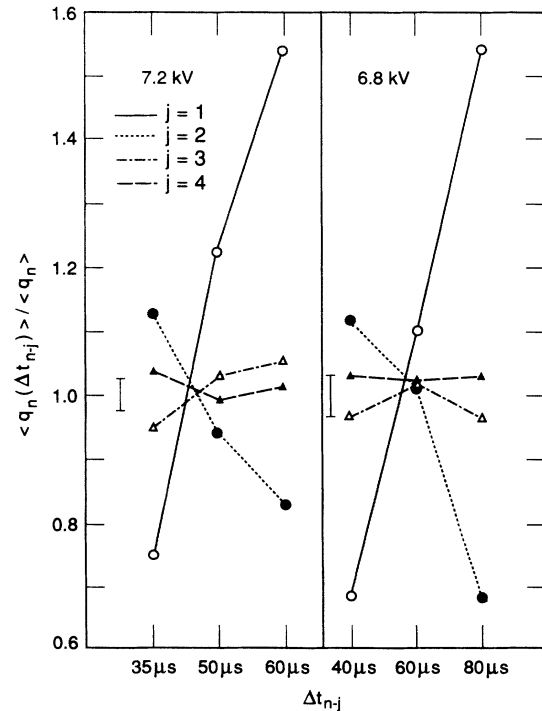


FIG. 23. Ratios of the expectation values $\langle q(\Delta t_{n-j}) \rangle / \langle q_n \rangle$ computed from the $p_1(q_n|\Delta t_{n-j})$ distributions shown in Fig. 22.

nomenon is a stochastic process in which memory effects play an important role. This phenomenon represents one of the clearest examples of a non-Markovian, marked random point process with stochastic properties that can be completely and unambiguously characterized by appropriate measurements. Any attempt to formulate a theoretical model that can account for regular Trichel-pulse behavior beyond the first pulse, i.e., for $n > 1$, must necessarily include effects of memory.

The stochastic properties of Trichel-pulse discharges determined here from the direct measurement of conditional and unconditional pulse-amplitude and time-separation distributions can be attributed to the influences of ion space charge and metastable species from previous pulses on the initiation and development of subsequent pulses. The predominant and most ubiquitous memory effect is that associated with the influence of the moving negative-ion space-charge cloud from the most recent pulse on the growth of the subsequent pulse. The influence of this space-charge cloud in suppressing the rate of initiating-electron release from the cathode is also evident in data from Ne+5% O₂. Mixtures that contain a higher relative O₂ concentration, i.e., N₂ + 20% O₂, Ne+95% O₂, and O₂, show indications of the influence of metastable species from earlier pulses on both the initiation and growth of subsequent pulses. One explanation for an increasing effectiveness of metastables in releasing electrons from the cathode with increasing O₂ content may be the corresponding higher fields required to initiate the discharge with consequent enhancements in field-assisted electron ejection by quenching of metastables on or near the cathode surface.

The unconditional pulse time-separation distributions exhibit well-defined critical minimum time separations Δt_c below which subsequent pulses do not occur. The minimum time separation determines the maximum pulse repetition rate that can occur under any given set of gap conditions and is physically more significant and better defined than the previously measured pulse repetition rate. For uv-sustained discharge pulses, Δt_c is independent of uv intensity but increases exponentially with decreasing gap voltage and evidently represents the time for restoration of the field near the cathode to a value required for initiation and development of the next pulse. This time is controlled by the ambipolar diffusion of ions produced during the most recent discharge event.

When discharge initiation is controlled predominantly by field-assisted photoelectron emission at the cathode, the pulse time-separation distributions exhibit tails at the high end that decrease exponentially at a rate which increases with increasing uv intensity and are consistent with a von Laue distribution. At low uv intensity, the unconditional pulse-amplitude distributions become sharply peaked at maximum values q_{lim} which increase with gap voltage and correspond to the largest pulses that can be formed in a gap free of space charge. The observed behavior of the unconditional pulse-amplitude and time-separation distributions are consistent with all

previously published data on the electrical characteristics of Trichel pulses.

Because of strong correlations that occur among pulse amplitudes and time separations, the conditional and unconditional pulse-amplitude and time-separation distributions have mutual dependences that can be predicted successfully using appropriate integral relationships that connect these distributions. The measured conditional distributions also give the required consistency in the signs of dependences between the pulse-amplitude and time-separation variables. Strong correlations were not only found between q_n and Δt_{n-1} , but also, in some cases, between q_n and q_{n-1} and between q_n and Δt_{n-2} for fixed Δt_{n-1} . Significant dependences of Δt_n on q_n and Δt_{n-1} were also found. From the measured conditional distributions $p_1(q_n|\Delta t_{n-j})$, correlations were shown to exist between q_n and all Δt_{n-j} , $j \leq 4$. Because of the dependences of q_n (or Δt_n) on Δt_{n-1} and q_{n-1} , "memory" can extend back to a large number of earlier events in a Trichel-pulse corona. Experimental limitations to verifying the extent of memory propagation by the present method have been analyzed.

In the present work, the discharge pulse amplitude was chosen as the "mark" that gives a measure of the discharge magnitude. There are other marks associated with other characteristics of the discharge pulse that could be considered. Amplitude was selected not only because it is a measure of discharge intensity but also because it can be measured easily. Other less easily measured marks such as the pulse shape parameters might also be correlated significantly with pulse-time separation as suggested by Morrow.¹⁸ Additionally, one could consider optical emission characteristics of the discharge. It should finally be noted that the measurement method applied here to investigate Trichel pulses could also be used to measure stochastic behavior in other types of pulsating or time-ordered phenomena that can be represented as random point processes for which the appropriate marks can be converted to electrical signals that increase in proportion to the magnitude of the mark.

ACKNOWLEDGMENTS

This work was supported in part by the U.S. Department of Energy, Office of Electric Energy Systems and in part by the National Institute of Standards and Technology. The authors are grateful to J. P. Steiner and A. V. Phelps for offering valuable suggestions.

APPENDIX

It was demonstrated from the results presented in Sec. IV E that for sufficiently large j , the profiles for the $p_1(q_n|\Delta t_{n-j})$ distributions become indistinguishable from the profile for the unconditional $p_0(q_n)$ distribution. The conditions under which this equality between p_1 and p_0 holds will now be examined for the case of a strong positive dependence of q_n on Δt_{n-1} . From the law of probabilities, the integral relationship for $p_1(q_n|\Delta t_{n-j})$ which applies in general for arbitrary $j > 1$, is

$$\begin{aligned}
& p_1(q_n | \Delta t_{n-j}) \\
&= \int_{\Delta t_{n-1}} \cdots \int_{\Delta t_{n-j+1}} \int_{q_{n-1}} \cdots \int_{q_{n-j+1}} p_1(q_{n-j+1} | \Delta t_{n-j}) p_2(\Delta t_{n-j+1} | q_{n-j+1}, \Delta t_{n-j}) \\
&\quad \times \prod_{i=2}^j p_{2i-1}(q_{n-j+i} | \{\Delta t_{n-k}, q_{n-k}\}, \Delta t_{n-j}) \\
&\quad \times \prod_{i=2}^{j-1} p_{2i}(\Delta t_{n-j+1} | q_{n-j+1}, \{\Delta t_{n-k}, q_{n-k}\}, \Delta t_{n-j}) \\
&\quad \times \prod_{i=1}^{j-1} dq_{n-i} d(\Delta t_{n-i}), \tag{A1}
\end{aligned}$$

where k assumes all integer values in the range

$$j - i + 1 \leq k \leq j - 1.$$

In the case of a strong $(q_n, \Delta t_{n-1})$ dependence as defined in Sec. II B, Eq. (A1) reduces to

$$p_1(q_n | \Delta t_{n-j}) = \int_{\Delta t_{n-1}} \cdots \int_{\Delta t_{n-j+1}} p_{2j-2}(q_n | \{\Delta t_{n-\ell}\}) \prod_{i=1}^{j-1} p_{2i-1}(\Delta t_{n-j+i} | \{\Delta t_{n-k}\}) d(\Delta t_{n-i}), \tag{A2}$$

where $\ell = 1, 2, \dots, j$ and $j - i + 1 \leq k \leq j$. In deriving Eq. (A2) from Eq. (A1) it is necessary to use the normalization condition Eq. (1).

Consider the following four special cases such as might be imposed by instrumental resolution.

Case 1:

$$\begin{aligned}
p_{2j-2}(q_n | \{\Delta t_{n-\ell}\}) &= p_2(q_n | \Delta t_{n-1}, \Delta t_{n-2}), \\
j &\geq 2, 1 \leq \ell \leq j. \tag{A3}
\end{aligned}$$

Case 2:

$$\begin{aligned}
p_{2j-2}(q_n | \{\Delta t_{n-\ell}\}) &= p_3(q_n | \Delta t_{n-1}, \Delta t_{n-2}, \Delta t_{n-3}), \\
j &\geq 3, 1 \leq \ell \leq j. \tag{A4}
\end{aligned}$$

Case 3:

and

$$p_1(\Delta t_{n-j+i} | \Delta t_{n-j+i-k}) = p_0(\Delta t_{n-j+i}) \tag{A6}$$

for all $k > 1$.

Case 4:

$$\begin{aligned}
p_{2i-1}(\Delta t_{n-\ell} | \{\Delta t_{n-k}\}) &= p_2(\Delta t_{n-\ell} | \Delta t_{n-\ell-1}, \Delta t_{n-\ell-2}), \\
\ell &= j - i \tag{A7}
\end{aligned}$$

and

$$p_2(\Delta t_{n-\ell} | \Delta t_{n-\ell-m}, \Delta t_{n-\ell-m'}) = \begin{cases} p_0(\Delta t_{n-\ell}) & \text{for } m \text{ and } m' \geq 3 \\ p_1(\Delta t_{n-\ell} | \Delta t_{n-\ell}) & \text{for } m = 1, m' \geq 3 \\ p_1(\Delta t_{n-\ell} | \Delta t_{n-\ell-2}) & \text{for } m = 2, m' \geq 3. \end{cases} \tag{A8}$$

Cases 1 (and 2) correspond, respectively, to situations where correlations between q_n and Δt_{n-3} (or q_n and Δt_{n-4}) either do not exist or cannot be experimentally ascertained. Likewise, cases 3 (and 4) correspond, respectively, to situations where correlations between Δt_n and Δt_{n-2} (or Δt_{n-3}) either do not exist or cannot be experimentally ascertained.

Inserting the combination of cases 1 and 3 into Eq. (A2) gives

$$p_1(q_n | \Delta t_{n-j}) = \int_{\Delta t_{n-1}} \cdots \int_{\Delta t_{n-j+1}} p_2(q_n | \Delta t_{n-1}, \Delta t_{n-2}) \prod_{i=1}^{j-1} p_1(\Delta t_{n-j+i} | \Delta t_{n-j+i-1}) d(\Delta t_{n-i}). \tag{A9}$$

Using the integral relationships

$$\int_{\Delta t_{n-i-1}} p_1(\Delta t_{n-i} | \Delta t_{n-i-1}) p_1(\Delta t_{n-i-1} | \Delta t_{n-i-2}) d(\Delta t_{n-i-1}) = p_1(\Delta t_{n-i} | \Delta t_{n-i-2}) = p_0(\Delta t_{n-i}) \tag{A10}$$

and

$$\int_{\Delta t_{n-1}} p_0(\Delta t_{n-i}) p_1(\Delta t_{n-i+1} | \Delta t_{n-i}) d(\Delta t_{n-i}) = p_0(\Delta t_{n-i+1}), \quad (\text{A11})$$

Eq. (A9) becomes

$$p_1(q_n | \Delta t_{n-j}) = \int_{\Delta t_{n-1}} \int_{\Delta t_{n-2}} p_0(\Delta t_{n-2}) p_1(\Delta t_{n-1} | \Delta t_{n-2}) p_2(q_n | \Delta t_{n-1}, \Delta t_{n-2}) d(\Delta t_{n-1}) d(\Delta t_{n-2}), \quad (\text{A12})$$

which is simply

$$p_1(q_n | \Delta t_{n-j}) = p_0(q_n), \quad (\text{A13})$$

provided $j \geq 4$.

Using the combination of cases 1 and 4 in Eq. (A2) together with the integral relationship

$$\begin{aligned} & \int_{\Delta t_{n-1}} p_1(\Delta t_{n-i} | \Delta t_{n-i-1}) p_2(\Delta t_{n-i+1} | \Delta t_{n-i}, \Delta t_{n-i-1}) \\ & \times p_2(\Delta t_{n-i+2} | \Delta t_{n-i+1}, \Delta t_{n-i}) d(\Delta t_{n-i}) \\ & = p_1(\Delta t_{n-i+2} | \Delta t_{n-i+1}) p_1(\Delta t_{n-i+1} | \Delta t_{n-i-1}) \end{aligned} \quad (\text{A14})$$

gives Eq. (A13) if $j \geq 5$. It can also be shown that the combination of case 2 with cases 3 and 4, respectively, give Eq. (A13) if $j \geq 5$ and 6. The above arguments can obviously be extended to cases where higher order correlations between q_n and Δt_{n-i} ($i > 3$) or between Δt_n and Δt_{n-i} ($i \geq 3$) can be distinguished. The combination of cases 1 and 3 correspond to the lowest order of correlations implied by the present experimental situation. Therefore $j = 4$ is the lowest j for which Eq. (A13) can be expected to apply, especially for the Ne+5% O₂ results presented here. This appears to be consistent with the data shown in Sec. IV E. The limitations on noise level in the measurement of higher-order conditional probability distributions for a time-ordered process has previously been noted by Packard and co-workers.⁶²

¹G. W. Trichel, Phys. Rev. **54**, 1078 (1938).

²G. L. Weissler, Phys. Rev. **63**, 96 (1943).

³L. B. Loeb, A. F. Kip, G. G. Hudson, and W. H. Bennett, Phys. Rev. **60**, 714 (1941).

⁴H. W. Bandel, Phys. Rev. **84**, 95 (1951); M. R. Amin, J. Appl. Phys. **25**, 627 (1954); M. K. Das, Z. Angew. Phys. **13**, 410 (1961).

⁵P. S. Gardiner, Proc. IEE **125**, 469 (1978).

⁶W. L. Lama and C. F. Gallo, J. Appl. Phys. **45**, 103 (1974).

⁷R. J. Van Brunt and D. Leep, J. Appl. Phys. **52**, 6588 (1981).

⁸C. Bugge, Norwegian Institute of Technology Technical Report No. EIP 68-1, 1969.

⁹W. N. English, Phys. Rev. **77**, 850 (1950).

¹⁰R. Zentner, Z. Angew. Phys. **29**, 294 (1970).

¹¹A. Schwab, Z. Angew. Phys. **17**, 52 (1964).

¹²M. Cernak and T. Hosokawa, Jpn. J. Appl. Phys. **26**, L172 (1987); **27**, 1005 (1988); Appl. Phys. Lett. **52**, 185 (1988); Jpn. J. Appl. Phys. **28**, 1989 (1989).

¹³J. A. Cross, R. Morrow, and G. N. Haddad, J. Phys. D **19**, 1007 (1986).

¹⁴D. A. Scott and G. N. Haddad, J. Phys. D **20**, 1039 (1987); **19**, 1507 (1986).

¹⁵S. V. Kulkarni and R. S. Nema, in *Conference Record of the 1988 IEEE International Symposium on Electrical Insulation, Cambridge, 1988* (IEEE, New York, 1988), pp. 364-367; S. V. Kulkarni and R. S. Nema, *Gaseous Dielectrics V, Proceedings of the Fifth International Symposium on Gaseous Dielectrics, Knoxville, 1987* (Pergamon, New York, 1987), pp. 637-642.

¹⁶L. B. Loeb, Phys. Rev. **86**, 256 (1952).

¹⁷L. B. Loeb, *Electrical Coronas—Their Basic Physical Mechanisms* (University of California, Berkeley, 1965).

¹⁸R. Morrow, Phys. Rev. A **32**, 1799 (1985).

¹⁹R. Morrow, Phys. Rev. A **32**, 3821 (1985).

²⁰R. Morrow and J. J. Lowke, J. Phys. D **14**, 2027 (1981).

²¹A. J. Davies and C. J. Evans, Proc. IEE **114**, 1547 (1967).

²²A. J. Davies, C. J. Evans, and F. Llewellyn-Jones, Proc. R. Soc. London Ser. A **281**, 164 (1964).

²³H. G. Stever, Phys. Rev. **61**, 38 (1942).

²⁴C. G. Montgomery and D. D. Montgomery, Phys. Rev. **57**, 1030 (1940).

²⁵J. P. Steiner, Ph.D. thesis, Purdue University, 1988 (unpublished).

²⁶N. H. Malik and A. A. Al-rainy, IEEE Trans. Electr. Insul. **EI-22**, 825 (1987); **EI-24**, 681 (1989).

²⁷R. J. Van Brunt and S. V. Kulkarni, Rev. Sci. Instrum. **60**, 3012 (1989).

²⁸R. J. Van Brunt and S. V. Kulkarni, in *Conference Record of the 1988 IEEE International Symposium on Electrical Insulation, Cambridge, 1988* (IEEE, New York, 1988), pp. 233-237.

²⁹S. V. Kulkarni and R. J. Van Brunt, in *Proceedings of the Ninth International Conference on Gas Discharges and Their Applications, Venice, 1988* (Benetton, Padova, 1988), pp. 227-230.

³⁰R. J. Van Brunt and S. V. Kulkarni, Bull. Am. Phys. Soc. **34**, 322 (1989).

³¹J. L. Melsa and A. P. Sage, *An Introduction to Probability and Stochastic Processes* (Prentice Hall, Englewood Cliffs, NJ, 1973), pp. 89-106. The notation adopted here for probability distributions (more properly referred to as

- probability density functions) differs somewhat from that given in this reference where, for example, the probability for any pulse to have amplitude between q_n and $q_n + dq_n$ might be more appropriately denoted by $p_{q_n}(x)dx$ instead of $p_0(q_n)dq_n$. Here x represents values assumed by the random variable q_n . The notation used in this text for conditional probabilities would also require that $p_1(q_n|\Delta t_{n-1})dq_n = p_{q_n|\Delta t_{n-1}}(x|y)dx$, where y represents the values assumed by Δt_{n-1} .
- ³²W. Feller, *An Introduction to Probability Theory and Its Applications* (Wiley, New York, 1968), Vol. 1, pp. 114.
- ³³D. L. Snyder, *Random Point Processes* (Wiley, New York, 1975), pp. 434-455; D. König and K. Matthes, *Math. Nachr.* **26**, 45 (1963); K. Matthes, *Jahresber. Dtsch. Math. Ver.* **66**, 66 (1963).
- ³⁴R. H. Fowler and L. Nordheim, *Proc. R. Soc. London Ser. A* **119**, 173 (1928).
- ³⁵J. W. Mason and B. Young, in *Proceedings of the Seventh International Conference on Gas Discharges and Their Applications, London, 1982* (Peregrinus, London, 1982), pp. 196-199.
- ³⁶Because it was not possible to precisely measure uv intensity at the cathode at any given time, the extent to which $|d[\log_{10} p_0(\Delta t_n)]/d(\Delta t_n)|$ was directly proportional to I_i could not be determined.
- ³⁷M. von Laue, *Ann. Phys. (Leipzig)* **76**, 721 (1925). [Also see R. V. Hodges, R. N. Varney, and J. F. Riley, *Phys. Rev. A* **31**, 2610 (1985).]
- ³⁸E. O. Lawrence and L. B. Linford, *Phys. Rev.* **36**, 482 (1930); L. B. Linford, *ibid.* **36**, 1100 (1930).
- ³⁹W. Schottky, *Z. Phys.* **14**, 63 (1923).
- ⁴⁰H. Bohringer, D. W. Fahey, W. Lindinger, F. Howorka, F. C. Fehsenfeld, and D. L. Albritton, *Int. J. Mass Spectrom. Ion Phys.* **81**, 45 (1987).
- ⁴¹S. A. Lawton and A. V. Phelps, *J. Chem. Phys.* **69**, 1055 (1978).
- ⁴²F. D. Findlay and D. R. Snelling, *J. Chem. Phys.* **55**, 545 (1971); F. D. Findlay, C. J. Fortin, and D. R. Snelling, *Chem. Phys. Lett.* **3**, 204 (1969).
- ⁴³I. D. Clark and R. P. Wayne, *Proc. R. Soc. London Ser. A* **314**, 111 (1969).
- ⁴⁴R. P. Steer, R. A. Ackerman, and J. N. Pitts, *J. Chem. Phys.* **51**, 843 (1969).
- ⁴⁵J. M. Thomas, F. Kaufman, and M. F. Golde, *J. Chem. Phys.* **86**, 6885 (1987).
- ⁴⁶L. G. Piper, G. E. Caledonia, and J. P. Kennealy, *J. Chem. Phys.* **74**, 2888 (1981).
- ⁴⁷M. M. Pejovic and B. J. Mijovic, *Zh. Tekh. Fiz.* **58**, 2129 (1988) [*Sov. Phys.—Tech. Phys.* **33**, 1290 (1988)].
- ⁴⁸M. A. Folkard and S. C. Haydon, *J. Phys. B* **6**, 214 (1973); S. C. Haydon and O. M. Williams, *ibid.* **6**, 227 (1973).
- ⁴⁹A. Yokoyama and Y. Hatano, *Chem. Phys.* **63**, 59 (1981).
- ⁵⁰A. Cardwell, *Phys. Rev.* **92**, 554 (1953).
- ⁵¹H. Kobayashi and S. Kato, *Surf. Sci.* **18**, 341 (1969).
- ⁵²R. J. Van Brunt, *J. Appl. Phys.* **59**, 2314 (1986).
- ⁵³W. Legler, *Z. Naturforsch.* **16A**, 253 (1961).
- ⁵⁴R. Geballe and M. L. Reeves, *Phys. Rev.* **92**, 867 (1953).
- ⁵⁵J. Gallagher, E. C. Beaty, J. Dutton, and L. C. Pitchford, *J. Phys. Chem. Ref. Data* **12**, 109 (1983).
- ⁵⁶D. K. Edwards, V. E. Denny, and A. F. Mills, *Transfer Processes* (McGraw-Hill, New York, 1978), pp. 38-68.
- ⁵⁷S. Yoshida, A. V. Phelps, and L. C. Pitchford, *Phys. Rev. A* **27**, 2858 (1983).
- ⁵⁸S. R. Hunter and L. G. Christophorou, in *Electron-Molecule Interactions and Their Applications*, edited by L. G. Christophorou (Academic, New York, 1984), Vol. 2, pp. 89-219.
- ⁵⁹F. M. Penning, *Physica* **8**, 137 (1928).
- ⁶⁰K. C. Smyth, R. A. Keller, and F. F. Crim, *Chem. Phys. Lett.* **55**, 473 (1978).
- ⁶¹D. Feldmann, *Opt. Commun.* **29**, 67 (1979).
- ⁶²N. H. Packard, J. P. Crutchfield, J. D. Farmer, and R. S. Shaw, *Phys. Rev. Lett.* **45**, 712 (1980).